

LONG WAVE INFRARED SCAN LENS DESIGN AND DISTORTION CORRECTION

by

Andy McCarron

Copyright © Andy McCarron 2016

A Thesis Submitted to the Faculty of the

DEPARTMENT OF OPTICAL SCIENCES

In Partial Fulfillment of the Requirements

For the Degree of

MASTER OF SCIENCE

In the Graduate College

THE UNIVERSITY OF ARIZONA

2016

ACKNOWLEDGEMENTS

Special thanks to Professor Jose Sasian for Chairing this Thesis Committee, and to Committee Members Professor John Grievenkamp, and Professor Matthew Kupinski. I've learned all lot from each of you through the years.

Thanks to Markem-Imaje for financial support.

Most importantly, I offer thanks and appreciation to my family for the support, encouragement, and patience along the way.

Table of Contents

Table of Figures	6
Table of Tables	10
Abstract.....	11
1. Background.....	12
1.1 Scanning System Overview	12
1.2 Scan Lens Prior Art.....	13
1.2.1 Telecentric Scan Lens	13
1.2.2 Conventional Scan Lens	13
1.2.3 F-Theta Scan Lens	14
1.2.4 Scan Lens Summary	14
1.3 Scan Lens Introduction	15
1.4 Scan Lens Design Overview.....	17
1.4.1 Introduction to Aberrations.....	18
1.4.2 Discussion of Aberrations.....	20
1.4.2.1 Defocus Aberration: W020	23
1.4.2.2 Spherical Aberration: W040	23
1.4.2.3 Coma Aberration: W131	24
1.4.2.4 Astigmatism Aberration: W222	25
1.4.2.5 Field Curvature Aberration: W220 and W220P	26
1.4.2.6 Distortion Aberration: W_{311}	26
1.4.2.7 Other Aberrations.....	27
1.4.3 Evaluation of Aberrations	29
1.4.4 Lens Coating	31
1.4.5 Lens Material	32
1.4.6 Correction Equation Development Overview.....	32
2. Scan Lens Design.....	35
2.1 Constraints and Requirements	37
2.2 Image Quality.....	39
2.2.1 Print Field.....	39
2.2.2 Irradiance: Peak and Uniformity.....	39
2.2.3 Distortion	40
2.3 Assumptions and Limitations	41
2.4 Modeling the Systems.....	41

2.4.1 Simplified System.....	41
2.4.1.1 Results.....	42
2.4.2 Scanning System.....	45
2.4.2.1 Results.....	45
2.4.2.2 Distortion Correction	47
2.4.3 Aspheric Scanning System	50
2.4.3.1 Results.....	50
2.4.3.2 Distortion Correction	52
2.4.4 F-Theta Simplified System	54
2.4.4.1 Results.....	54
2.4.5 F-Theta Scanning System	57
2.4.5.1 Results.....	58
3. Conclusion	61
Appendix.....	63
A1: Useful Equations.....	63
Wavelength and Frequency Relation.....	63
Diffraction Limited Spot Size.....	63
Lens Power and Focal Length (Lens Makers Formula for a Thick Lens in Air).....	63
Surface Power	63
Surface Sag	64
Back Focal Distance	64
RMS Spot Size (15)	64
Lens Shape Factor.....	64
A2: Seidel Coefficients.....	65
A3: Optic Studio Macro for Print Field Distortion.....	66
Works Cited	69

Table of Figures

Figure 1: Multiple views of a dual axis scanning system. The green cylinder represents the beam path. The X Scanner controls the first mirror along the beam path, the Y Scanner controls the second mirror.	12
Figure 2: The 3 most common types of scan lenses (telecentric, conventional, and F-Theta) compared to a regular meniscus lens (3).....	13
Figure 3: Image size and with respect to input angle for a Conventional and F-Theta scan lens.	15
Figure 4: Conventional scan lens cross section with on axis incident beam and illustrative geometry. Key terminology has been labeled. The lens mount is shown in blue.....	15
Figure 5: Scan lens diagram with superimposed beams scanned by the X (red beam) and Y (black beam) mirror. The Y beam would be scanned perpendicular to the page, but is shown parallel for comparison purposes. All dimensions are arbitrary. The lens mount is shown in blue.	17
Figure 6: Frequency wavelength relation. A high frequency (solid lines) results in a short wavelength (dotted lines).....	18
Figure 7: Collimated monochromatic light with planar wavefronts (far left) incident on a lens resulting in converging light with spherical wavefronts (right of lens). Rays and wavefronts are orthogonal.	18
Figure 8: Overview of how aberrations can be categorized and evaluated by different attributes (9).....	19
Figure 9: Aberrations that effect scan lens design, and their azimuthal angle, field height, and Pupil height dependence. (11).....	20
Figure 10: The reference sphere and ray (maroon) compared to the paraxial ray (blue). The diagram above shows an under corrected system.	23
Figure 11: Spherical aberration and its effect on spot size. (9)	24
Figure 12: Coma occurs when the focal plane shifts with lens radius (Zones) and field of view. There is no Coma on axis. (16) The system to the far right shows how coma decreases with field position.....	24
Figure 13: Astigmatism, and Field Curvature. Blue represents the rays in the tangential plane (T), green in the sagittal (S). The black line represents the medial (M) imaging surface where the smallest spot size is realized. The maroon line indicates the Petzval (P) surface. Dotted lines indicate the ideal focal location at the specific field of view shown; solid lines show the ideal focal location over the entire field of view (Side View Only). The Image Plane View shows what the spot diagram would like at the specific field of view.	25

Figure 14: Simplified depiction of distortion in a Conventional scan lens.....	26
Figure 15: Example of Geometric Distortion over a 250x250mm. Polar: Green arrow indicates tangential, black arrow indicates radial distortion. Cartesian: Blue arrow indicates Y, purple arrow indicates X distortion. (directions shown are arbitrary)	27
Figure 16: A meniscus scan lens diagram for ray tracing (top) and represented as a simplified Gaussian system (bottom). In both systems the chief (green) and marginal (maroon) are shown off axis and passing parallel through the stop.....	29
Figure 17: The effect of bending the lens on total system aberrations at the maximum object field of view (the curvature of both surfaces increase from left to right)	30
Figure 18: The effect of bending the lens and the aberrations introduced at each surface. Solid lines denote first surface, dotted lines denote second surface.	31
Figure 19: Correction Equation development flow chart.	34
Figure 20: Overview of the Systems designed and their progression.....	36
Figure 21: Tunnel diagram of scan lens design parameters (solid black line denotes the beam path, dotted line represents a length of the beam path can be used as an optimization parameter).	38
Figure 22: Print field size and shape requirements.....	39
Figure 23: Layout for the <i>Simplified System</i> . Fields are represented by different colored ray bundles.	42
Figure 24: Aberrations as each surface of the <i>Simplified System</i> Scale is 20um / horizontal bar. The max total distortion is ~0.1 mm.....	43
Figure 25: Diffraction encircled energy of the <i>Simplified System</i> compared to the diffraction limit. The system is within 1% at the print field center and 13% at the print field corner	43
Figure 26: Huygens PSF Spot Irradiance of the <i>Simplified System</i> (left), spot diagrams displayed with the Airy disk at the image center (top right), and corner (bottom right)	44
Figure 27: POP results for spots at the center (left) and corner (right) of the <i>Simplified System</i> image field.	44
Figure 28: Layout for the <i>F-Theta Scanning System</i> . Configurations are represented by different colored ray bundles. The incident beam starts perpendicular to the page. Drawings to right show close up of X (green) and Y (pink) mirrors.	45
Figure 29: Diffraction encircled energy of the <i>Scanning System</i> compared to the diffraction limit. The system is within 1% at the print field center and 10% at the print field corner.....	46

Figure 30: Huygens PSF Spot Irradiance of the <i>Scanning System</i> (left), spot diagrams displayed with the Airy disk of the rays at the print field center (top right), and corner (bottom right)	46
Figure 31: POP results for spots at the center (left) and corner (right) of the <i>Scanning System</i> print field.....	47
Figure 32: Diagram illustrating the conversion of position to angular distortion.....	47
Figure 33: <i>Scanning System</i> ideal print field overlaid with distorted and corrected image. The magnification factor was adjusted to minimize the error in the + shaped print field. This came at the cost of increasing the error for the spots located outside the desired print field which would be vignetted by the lens mount aperture (black circle)	49
Figure 34: Accuracy of the corrected <i>Scanning System</i> along the print field edges.....	49
Figure 35: X and Y curvature of the aspheric as seen by the on-axis configuration.	50
Figure 36: Diffraction encircled energy of the <i>Aspheric Scanning System</i> compared to the diffraction limit. The system is within 1.0% at the print field center and 6.0% at the print field corner.	51
Figure 37: Huygens PSF cross sections of Spot Irradiance (left), spot diagrams displayed with the Airy disk of the rays at the print field center (top right), and corner (bottom right) for the <i>Aspheric Scanning System</i>	51
Figure 38: POP results for spots at the center (left) and corner (right) of the <i>Aspheric Scanning System</i> print field.....	52
Figure 39: <i>Aspheric Scanning System</i> ideal print field overlaid with distorted and corrected image. The magnification factor was adjusted to minimize the error in the + shaped print field. This came at the cost of increasing the error for the spots located outside the desired print field which would be vignetted by the lens mount aperture (black circle)	53
Figure 40: Accuracy of the corrected <i>Aspheric Scanning System</i> along the print field edges.....	53
Figure 41: Layout for the <i>F-Theta Simplified System</i> . Fields are represented by different colored ray bundles.....	54
Figure 42: Aberrations at each surface of the <i>F-Theta Simplified System</i> Scale is 200um / horizontal bar. The max total distortion is ~1.6 mm, the net sum is ~0.4 mm at the image.....	55
Figure 43: Diffraction encircled energy of the <i>F-Theta Simplified System</i> compared to the diffraction limit. The system is within 1% at the print field center and 5.0% at the print field corner	55
Figure 44: Huygens PSF Spot Irradiance (left), spot diagrams displayed with the Airy disk of the rays at the print field center (top right), and corner (bottom right).....	56

Figure 45: POP results for spots at the center (left) and corner (right) of the *F-Theta Simplified System* print field..... 56

Figure 46: Layout for the *F-Theta Scanning System*. Configurations are represented by different colored ray bundles. The incident beam starts perpendicular to the page. 57

Figure 47: Diffraction encircled energy of the *F-Theta Scanning System* compared to the diffraction limit. The system is within 0.5% at the image print field center and 3.5% at the corner 58

Figure 48: Huygens PSF Spot Irradiance (left), spot diagrams displayed with the Airy disk of the rays at the print field center (top right), and corner (bottom right) for the *F-Theta Scanning System*. 59

Figure 49: POP results for spots at the center (left) and corner (right) of the *F-Theta Scanning System* print field..... 59

Table of Tables

Table 1: Summary of scan lens attributes	14
Table 2: Aberration relevant to scan lens design. (12) (7).....	22
Table 3: Aberration not relevant to scan lens design.....	27
Table 4: Properties of common LWIR lens materials (21).....	32
Table 5: Summary of Systems that were designed and evaluated.....	35
Table 6: Scan lens requirements, and constraints for all systems.....	37
Table 7: Physical lens requirements	37
Table 8: Optimal geometry for the <i>Simplified System</i>	42
Table 9: Sum of Aberrations in the <i>Simplified System</i> at the image.....	42
Table 10: Optimal geometry for the <i>Scanning System</i>	45
Table 11: Correction equation polynomials and their coefficients for the <i>Scanning System</i>	48
Table 12: Optimal geometry for <i>Aspheric Scanning System</i>	50
Table 13: Correction equation polynomials and their coefficients for the <i>Aspheric Scanning System</i>	52
Table 14: Optimal geometry for <i>F-Theta Simplified System</i>	54
Table 15: Sum of Aberrations in the <i>F-Theta Simplified System</i> at the image.....	54
Table 16: Results of the <i>F-Theta Simplified System</i> with respect to the F-Theta criteria.....	57
Table 17: Optimal geometry for the <i>F-Theta Scanning System</i>	58
Table 18: Results of the <i>F-Theta Scanning System</i> with respect to the <i>f</i> -Theta criteria.	60
Table 19: Summary of System performance	61
Table 20: Seidel Coefficients (7)	65

Abstract

The objective of this Thesis is to design a scan lens for a long wave infrared laser marking system. The system is comprised of a laser source emitting a collimated beam coupled with a 14mm aperture dual axis galvanometer scanning system capable of scanning a range $\pm 11^\circ$ (mechanical). Multiple scan lens options will be considered. Each scan lens will be optimized to maximize peak irradiance and operate at, or near, the diffraction limit over a 210x110 mm ‘plus’ shaped field. Unintended distortion evident in some lens designs and will be compensated for by developing equations that allowed the proprietary imaging algorithm to adjust the angle of the scanning mirror appropriately to achieve an undistorted image. The accuracy of the distortion correction will be within 1% of the shortest image dimension.

Commercially available scan lenses are designed for generic scanning systems with no apriori knowledge of the imaging model and are typically available in arbitrary focal length increments. As a result, use of off the shelf scan lenses result in sub-optimal performance.

This thesis presents background information on galvanometer based scanning systems followed by a review of classical scan lenses. The imaging application and systems constraints for the marking system are defined. The steps taken to design and optimize a conventional, aspheric, and F-Theta scan lens are described, and their performances are compared with respect to the design requirements.

The Conventional scan lens coupled with a distortion correction equation was found to offer the best performance to cost ratio and was deemed the most appropriate lens for the marking system.

1. Background

1.1 Scanning System Overview

The application covered by this paper utilizes a dual axis galvanometer scanning system for a collimated long wave infrared laser source. The parameters of the laser source are presented in the later section. The functionality of the scanning system is independent of the laser source with the exception of the mirror coatings and the scan lens glass material.

A dual axis scanning system consists of 2 mirrors mounted on galvanometers connected to a servo control board. Galvanometers are small motors that are capable of being tuned to move a mirror in either fixed increments, or a continuous motion over a defined range. Galvanometers are typically confined to a rotation of $\pm 25^\circ$ (mechanical) or less, and the mirrors are typically capable of scanning a range of $\pm 11^\circ$ (mechanical), and as with any mirror, the beam deflection (optical angle) is twice the mechanical angle of rotation.

The galvanometers are mounted in the system such that the rotational axes of the mirrors are perpendicular to each other. This allows the mirrors to direct an incident beam in 2 directions, each independently of the other.

Scanning systems may locate the scan lens before or after the scanners (1). The system evaluated by this Thesis requires the scan lens be placed after the scanners. The primary function of the scan lens is to focus the incident beam to a flat imaging plane. (2) The scan lens will be described in more detail in the next section. The schematic of a dual axis scanning system is shown in the figure below.

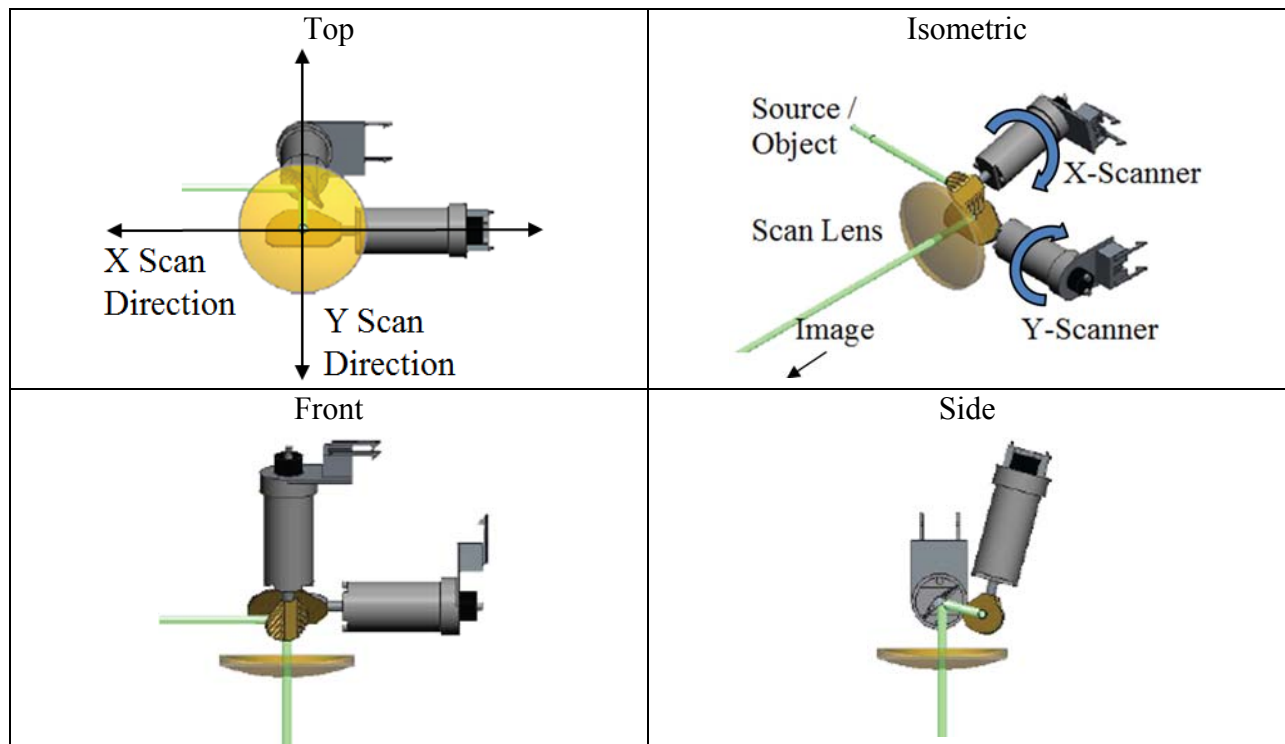


Figure 1: Multiple views of a dual axis scanning system. The green cylinder represents the beam path. The X Scanner controls the first mirror along the beam path, the Y Scanner controls the second mirror.

The key elements that were considered during the design and evaluation of the scanning systems included the location and sizes (linear or angular) of the object, pupils, system stop, principal planes and Image along with the resulting chief and marginal rays. The key elements of a scanning system are slightly unique, compared to other imaging systems. Insight into the scan lens system parameters will be presented in the following review.

1.2 Scan Lens Prior Art

For this report a scan lens will be defined as a lens used to focus a collimated beam to a flat imaging field. The focused beam creates a spot¹. The position of the spot on the image plane is controlled by adjusting the angle of the scan mirrors prior to the lens. A key distinction between a scan lens other lenses is the requirement of flat imaging plane.

Scan lenses are divided into categories based on specific attributes. The three most common categories that will be discussed in this paper are: Telecentric, Conventional (F-tan(Theta)), and F-Theta.

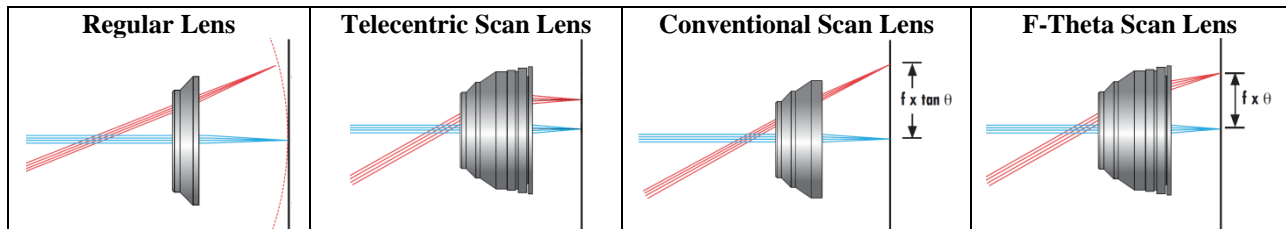


Figure 2: The 3 most common types of scan lenses (telecentric, conventional, and F-Theta) compared to a regular meniscus lens (3).

1.2.1 Telecentric Scan Lens

A Telecentric scan lens is a multi-element lens system designed to output the chief ray perpendicular to the image plane over the entire field of view. The main advantage of a Telecentric lens is the uniform spot size across the image field with no elliptical distortion from a non-orthogonal chief ray. The primary drawback of a Telecentric lens for scanning applications is lens size, which must equal or exceed that of the required image field size. For the scanning application discussed in this report the lens diameter would be approximately 280 mm which would make this lens far too bulky and costly to manufacture. The telecentric lens also requires multiple elements which would add additional cost and complexity. Telecentric lenses are more commonly used for imaging onto sensors when high resolution is required.

1.2.2 Conventional Scan Lens

A conventional scan lens is designed to create a flat imaging field with a nonlinear relationship between the object angular field of view and the location of the spot on image plane. In a distortion free system the relationship between incident angle and spot displacement is proportional to the focal length and can be calculated with the equation below: (4)

¹ The focused beam on the image plane will be referred to as a “spot” throughout this paper.

$$H = f * \tan \theta$$

where:

H	[mm]	Spot displacement (height)
f	[mm]	Focal length
θ	[rad]	Object incident angle (optical scan angle)

For the long wave infrared (LWIR) application cover by this paper the Conventional scan lens can be a single element positive meniscus lens or multi element doublet or triplet lens. The doublets and triplets give additional design parameters that allow the beam to focus closer to the diffraction limited spot size. The advantages of the multi-element lenses fall off with the focal length. (5) The performance increase of the multi element scan lenses comes at a cost premium. The material and coating cost are the two main contributors to the total lens cost². Doublets cost approximately two times a singlet and triplets cost approximately three times a singlet. The mounting part cost and assembly complexity also increases with the number of elements.

1.2.3 F-Theta Scan Lens

An F-Theta lens is similar to a conventional scan lens but is designed for a linear displacement of the spot on the image plane relative to the deflection of the scan mirrors. The relationship is shown in the equation below: (4)

$$H = f * \theta$$

where:

H	[mm]	Spot displacement (height)
f	[mm]	Focal length
θ	[rad]	Object incident angle (optical scan angle)

The near linear relation between the beam deflection and the beam translation simplifies the imaging algorithm. F-Theta lenses can be a single element positive meniscus lens or multi element doublet or triplet lenses. The performance and cost of the multi element F-Theta lenses are the same as discussed for Conventional Scan Lenses.

1.2.4 Scan Lens Summary

The characteristics of the different scan lens categories are presented below. The summary assumes the lenses have the same focal length, object field of view (scan mirror deflection), and incident beam diameter.

	Irradiance Uniformity Across Image	Print Field Size	Spot Displacement Distortion
Telecentric	Best	Smallest	Non-Linear
Conventional	Worst	Largest	Non-Linear
F-Theta	Middle	Middle	Linear

² The lens is assumed to be produced in large (>200) quantities, thus the initial tooling set-up and cost would be small relative to the material and coating cost on a per lens basis.

Both the Conventional and F-Theta scan lens would be a good fit for the application reviewed in this paper. A preliminary comparison of the Conventional and F-Theta scan lens indicate that the conventional lens would cover the required field with a smaller focal length resulting in higher peak irradiance but with less uniformity across the field. Given the initial design constraints to maximize both peak irradiance, and irradiance uniformity, both types of scan lenses will be designed and optimized to allow their performances to be compared.

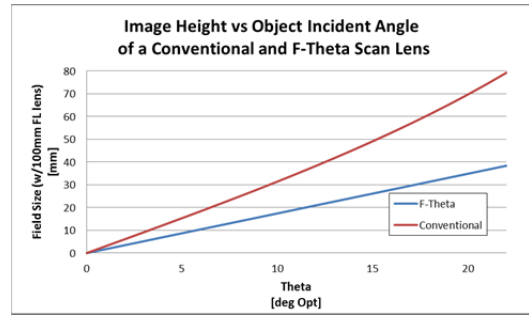


Figure 3: Image size and with respect to input angle for a Conventional and F-Theta scan lens.

1.3 Scan Lens Introduction

The diagram shown below depicts a Conventional positive meniscus scan lens typical of applications involving LWIR (CO₂) lasers. A positive meniscus lens, as opposed to a negative meniscus lens, is thicker in the center and thinner towards the edges due to a smaller radius on the convex surface compare to the radius on the concave surface. In keeping with the conventional optic standards, the diagram below is shown with light traveling from left to right. Both the convex and concave surfaces would have negative radii. The power of the first surface would be negative due to a change in medium from air ($n = 1$) to glass ($n \sim 2.4$) and the negative radius, and the power of the second surface would be positive due to the change in medium from glass to air and the negative radius³.

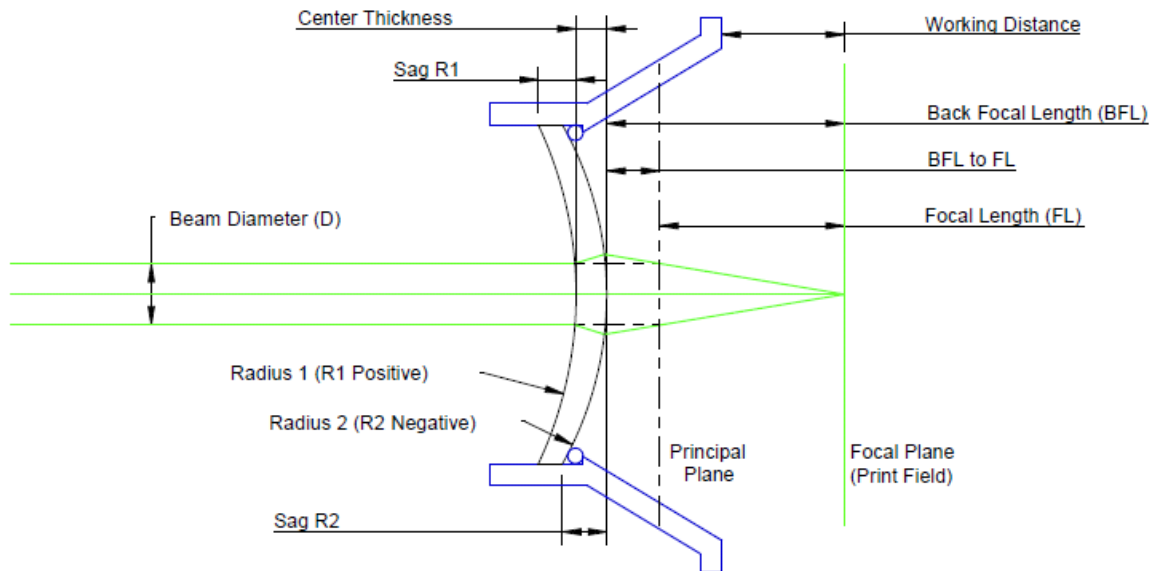


Figure 4: Conventional scan lens cross section with on axis incident beam and illustrative geometry. Key terminology has been labeled. The lens mount is shown in blue.

Practical definitions for a scanning system are described below:

³ See Appendix A1 for surface power equation

Principal Plane: The principal plane shown in the diagram is the rear principal plane of the system. The principle plane is the plane at which the collimated beam from the source would appear to start converging (as shown) or diverging. This also the plane of unit magnification.

Focal Length: The focal length is the distance from the principal plane to the focal plane. The Lens Makers formula to calculate the focal length is included in Appendix A1.

Focal Plane: The focal plane is the location where the beam is focused using equations derived from Gaussian optics.

***Image Plane (or The Effective Focal Plane):** The Image or Effective Focal Plane is not shown in the diagram. The effective focal plane is the plane at which a specific parameter is optimal; its distance is measured from the principal plane. This functionality is integrated into most ray trace software.

Spot (Image of the Laser Beam): The spot is the conjugate image of the collimated laser beam. The spot is located the focal plane and can be translated across the focal plane by changing the orientation of the mirrors.

Print Field: The print field is the area over which the spot can be located. The location of the spot is controlled by the scanning mirror orientation. During the scan lens review in prior sections this was referred to as the *Image Field*.

Back Focal Length: The Back focal Length is the distance from the vertex of the second surface to the focal plane.

Working Distance: The working distance is generally defined as the distance from the focal plane to a convenient surface that is fixed relative to the optical system. The lens mount is often used as a point of reference.

Surface Sag: The surface sag is the distance from the vertex of a lens to the plane defined by where the surface intersects the diameter of the lens. The surface sag can be calculated by the equation in Appendix A1.

Center Thickness: The center thickness is the distance from the vertex of the first surface to the vertex of the second surface along the optical axis.

Object: The object is a collimated, single mode, laser. The diameter of the laser can be used as the entrance pupil diameter when calculating the F-Number (1). The laser will be modeled in ray trace software as a monochromatic point source at infinity with the entrance pupil diameter used to define the beam diameter (or height).

F-Number (or F-Stop): The F-Number of a scanning system is defined as the ratio of the focal length divided by the beam input diameter. The beam input diameter (typically the $1/e^2$ value) is used instead of the stop because the stop is not well defined in a scanning system. The optical path should be designed such that the $1/e^2$ beam diameter is maintained throughout the system (minimum clear aperture of all components except scan mirrors is 1.5x the beam diameter). (6)

Stop: The stop in an optical system is generally defined as the limiting aperture. The stop location and diameter are parameters that can be used to control the amount of light passing through the system as well as the depth of field. The system stop in a scanning system is not well defined. In the scanning system the amount of light passing through the system is fixed by the incident laser beam (which affects the depth of field by defining the entrance pupil). The field of view is defined by the scanner rotation angles.

In geometric optics, the image and the stop are used to define the path of the chief ray and marginal ray. In a scanning system it is more appropriate to define the chief ray as coincident to the incident beam axis and the marginal ray as parallel to the chief ray displaced by the radius of the beam. Using this concept for the chief and marginal ray both the X and Y mirrors act as independent stop locations with respect to defining the field of view (due to the difference in location of the mirrors along the optical path). The Y mirror shown in the figure below deflects the beam perpendicular to the sheet of paper, and due to the difference in location from the X mirror, creates an asymmetric field of view. The figure below illustrates this effect, note how the field of view, as defined by the image height, is different for both X and Y, despite both mirrors deflecting the beam over the same angular field of view.

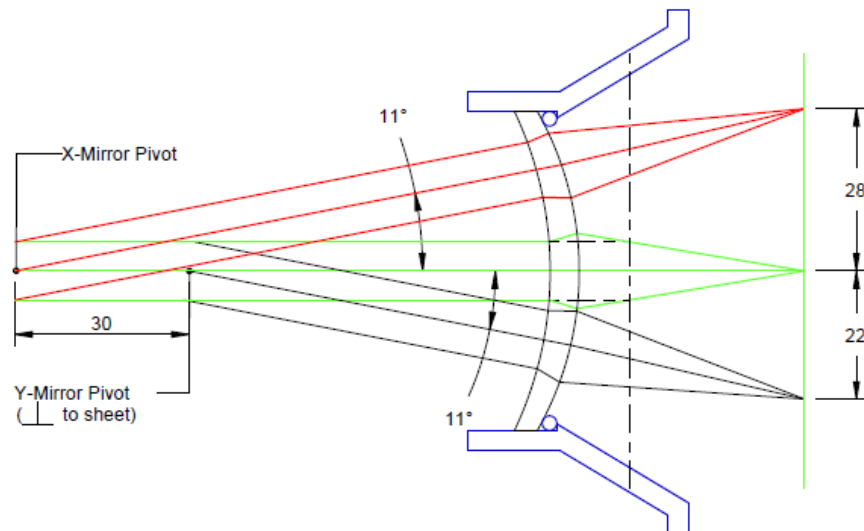


Figure 5: Scan lens diagram with superimposed beams scanned by the X (red beam) and Y (black beam) mirror. The Y beam would be scanned perpendicular to the page, but is shown parallel for comparison purposes. All dimensions are arbitrary. The lens mount is shown in blue.

Scan lens systems are often simplified in optical modeling programs by replacing both mirrors with a stop midway between the two mirrors. This simplification creates an axially symmetric model that is easier to set-up and optimize with the software.

1.4 Scan Lens Design Overview

A well designed scan lens will create a flat image field and operate at, or near, the diffraction limit for all locations across the image plane⁴. A spot diameter approaching the diffraction limit

⁴ See Appendix A1 for diffraction limited spot size equation

can be achieved by minimizing the wavefront error and appropriately selecting the image plane location.

1.4.1 Introduction to Aberrations

Light is a form of electromagnetic radiation, and has wave-like properties. The wave-like properties can be quantified based on frequency or wavelength both of which are related by the speed of light in a vacuum⁵.

A laser produces collimated, monochromatic, coherent light. This means all the waves of light are traveling parallel to each other (collimated) with the same frequency (monochromatic) and are in phase with each other (coherent) with planar wavefronts. The lens introduces a change in phase to the wavefronts which causes the beam to converge. The change in wavefront can be evaluated by analyzing the wavefront directly, or by tracing rays perpendicular to the wavefront (7) (8). The methods are redundant, as they are different ways to evaluate the same effect. Both methods have advantages in different situations and neither method accounts for diffraction effects⁶. In this report ray tracing will be the primary method used for the design of the scan lens. The final design will be evaluated with methods that take diffraction into consideration.

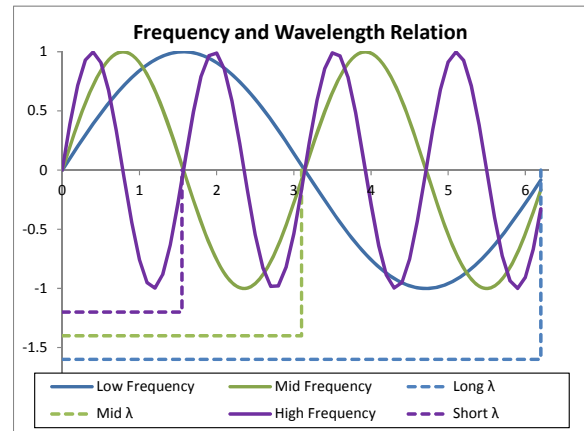


Figure 6: Frequency wavelength relation. A high frequency (solid lines) results in a short wavelength (dotted lines).

Historically, the surface of a lens starts as a plane or sphere and increases in complexity as needed to meet an application (this is done to minimize manufacturing and inspection costs). A spherical lens will naturally focus light to a spherical imaging surface. This must be overcome for the scan lens design, which requires a flat imaging surface, by introducing and balancing aberrations and image plane location against the spot size over the imaging field.

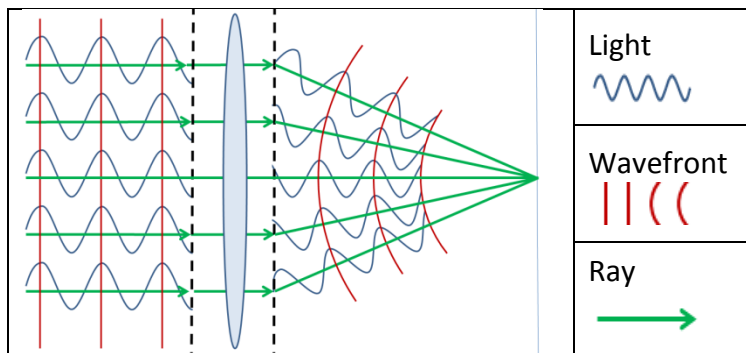


Figure 7: Collimated monochromatic light with planar wavefronts (far left) incident on a lens resulting in converging light with spherical wavefronts (right of lens). Rays and wavefronts are orthogonal.

The ideal spot on the imaging plane would be a point. To obtain a point, wavefronts must converge to the same location. The ideal wavefront shape to achieve a point on the image plane is a sphere. In practice the wavefront will exhibit some deviation from the perfect sphere and this deviation is categorized as an aberration.

Aberrations can be evaluated directly using data from ray tracing. This is

⁵ See Appendix A1 for wavelength to frequency equation

⁶ Diffraction is the effect of light bending, and spreading around the edge of apertures.

accomplished by comparing the calculated ray trace data to the theoretical data (that all rays should converge to a point, i.e. wavefronts are perfect spheres). The ideal lens will cause all the rays to intersect at the same location on the image plane. In practice, there will be some deviation in the ray location relative to the ideal location and this can be measured by observing angular, transverse, or longitudinal deviation of the ray.

The angular deviation of the ray is the angular offset of the ray relative to the angle of the ideal ray. The transverse deviation of a ray is the perpendicular offset of the ray location from the ideal location on the image plane. The spot size can be determined by measuring the root mean square (RMS) transverse deviation of all traced rays relative to either the Chief ray or Centroid⁷. The longitudinal deviation is the offset in the image plane location that would be required for the ray to reach the ideal location on the image plane.

Aberrations are measured in terms the optical path difference (OPD) between the actual and ideal spherical wavefront. The units of the OPD can be in waves, distance (spatial), or time (temporal). The diagram below visually depicts the different ways of assessing and viewing aberrations.

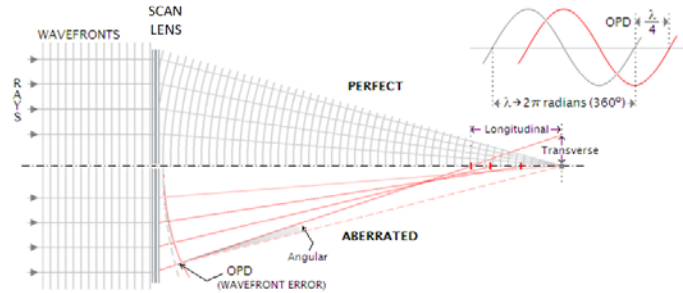


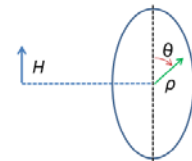
Figure 8: Overview of how aberrations can be categorized and evaluated by different attributes (9)

Aberration theory categorizes wavefront errors based on how they occur and their effect on image quality. This topic will be covered in more detail in a subsequent section. Tracing rays through the system provides a convenient way to determine the type and magnitude of the aberrations at each interface. The total aberration of the system is the sum of all contributing components through the system and can be derived from the equation below (7):

$$W_{Total} = \sum_{j,m,n} W_{k,l,m} (\vec{H} \cdot \vec{H})^j (\vec{H} \cdot \vec{\rho})^n (\vec{\rho} \cdot \vec{\rho})^m$$

where:

- W_{Total} The total aberration of the system at a location along the beam path
- $W_{k,l,m}$ The aberration coefficient at conditions described by k, l, m
- j Algebraic power for field of view contribution
- n Algebraic power of aperture contribution
- m Algebraic power of angular contribution
- k An integer to identify the aberration coefficient: $k = 2j + m$
- l An integer to identify the aberration coefficient: $l = 2n + m$
- H Normalized field height (1 is the edge of the field) can be defined with respect to the object or image
- ρ The normalized pupil radial extent (1 is the edge of the pupil)
- θ Azimuthal pupil coordinate between H and ρ



⁷ In this paper the Centroid will be used as the reference for RMS spot size and spot location. The centroid is located at the center of the highest ray density, making it the anticipated location of the peak spot intensity. The equation to calculate RMS spot size is in Appendix A1.

1.4.2 Discussion of Aberrations

The primary aberrations in most optical systems include: defocus, chromatic, and “third order” or Seidel⁸ aberrations. (10) The scan lens design is for monochromatic light and therefore chromatic aberrations do not need to be considered⁹. The Seidel aberrations include: spherical, coma, astigmatism, distortion and field curvature, all of which, in addition to defocus will be important to consider in the scan lens design. The dependence of the aberrations on field height, pupil height, and the azimuthal angle is shown in the Figure below.



Figure 9: Aberrations that effect scan lens design, and their azimuthal angle, field height, and Pupil height dependence. (11)

Defocus affects the longitudinal location of the image plane, and distortion affects the transverse location of the spot on the image plane, neither of which affects the convergence of the wave front (each spot across the image field is formed optimally, but not necessarily on the image plane or in the expected rectilinear location). In either case the ray trace data describes the image with respect to these aberrations completely and accurately. The remaining aberrations affect the convergence of the wavefronts resulting in changes to the spot footprint across the image field.

To evaluate the Seidel Aberrations both the ray trace data and information pertaining to the physical components in the system are needed. More detail on the Seidel Aberrations will be presented in a later section.

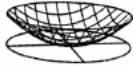
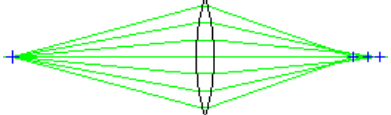
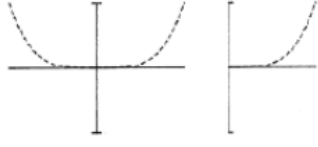
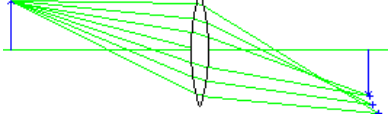
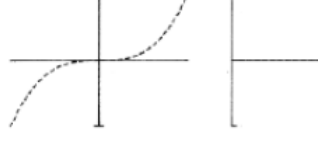
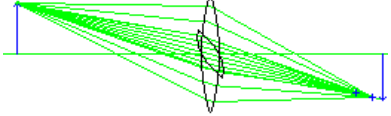
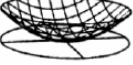
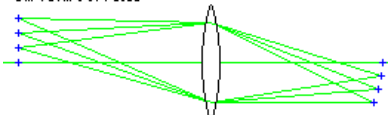
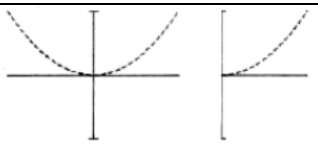
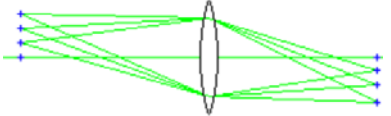
The aberrations shown in the table below show the rays focusing before the desired image plane. Systems with aberrations causing premature focus are termed under corrected. Alternatively, an over compensated systems results when the aberrations cause the rays to focus after the image plane. The effect of over compensation can be visualized by mirroring the aberration diagram and OPD fans about the image plane (horizontal axis) in the table below.

⁸ The “order” of an aberration stems from an algorithm with dependence on the powers of the pupil and angular dependence of the aberrations. The algorithm used to determine the order varies with method used to model the aberration (i.e Waveform expansion, Zernike, etc.).

⁹ Ultra-fast pulsed lasers (<20 ps) require inclusion of chromatic effects in the scan lens design due to the spectral width of the pulse (28)

There are special cases when the wavefront error for a particular aberration goes to 0 over the entire image field. An aplanatic system has no spherical or coma aberration and an anastigmatic system no spherical, coma, or astigmatism aberrations. The key design techniques that allow these systems to mitigate aberrations will be applied to the scan lens design.

An overview of the relevant aberrations and their effect on the scan lens design are presented in the table below.

Table 2: Aberration relevant to scan lens design. (12) (7)			
Aberration Syntax Effect on Image	Effect on Rays	Wavefront Error OPD Fan (tangential, sagittal)	Effect on lens design
Defocus $W_{020} \approx \rho^2$ 	The reference sphere radius is changed, thus affecting where rays focus along the optical axis <i>0th Order, On axis and off axis</i>		<ul style="list-style-type: none"> Used to locate the spot on the desired observation plane
Spherical $W_{040} \approx \rho^4$ 	Spherical Aberration  <i>3rd Order, On axis and off axis</i>		<ul style="list-style-type: none"> Bending lens can reduce error Aspheric surfaces can reduce error Splitting the lens can reduce error
Coma $W_{131} \approx H\rho^2 \cos \theta$ 	Coma  <i>3rd Order, Off axis only</i>		<ul style="list-style-type: none"> Bending lens can reduce error Adjusting stop location can reduce error Aspheric surfaces can reduce error Symmetry about the stop is not possible for the scan lens
Astigmatism $W_{222} \approx H^2\rho^2 \cos^2 \theta$ 	Astigmatism  <i>3rd Order, Off axis only</i>		<ul style="list-style-type: none"> Bending lens can reduce error Adjusting stop location can reduce error Aspheric surfaces can reduce error Can be balanced with Field Curvature
Field Curvature $W_{220} \approx H^2\rho^2$ 	Curvature of Field  <i>3rd Order, Off axis only</i>		<ul style="list-style-type: none"> Bending lens can reduce error The index of refraction is fixed due to selection of base material Can be balanced with astigmatism
Distortion $W_{311} \approx H^3\rho^2 \cos \theta$ 	Distortion  <i>3rd Order, Off axis only</i>	Only affects location of spot on image plane, no effect on wavefront error	<ul style="list-style-type: none"> This can be compensated with a correction equation applied to the scanners This can be manipulated to achieve a specific relationship between object incident angle and image height

1.4.2.1 Defocus Aberration: W_{020}

Defocus is also a second order term with quadratic dependence on the aperture. The paraxial ray trace defines the reference sphere perfectly, and therefore when using the reference sphere, there is no defocus aberration ($W_{020} = 0$). Introducing a non-zero value for the defocus term ($W_{020} \neq 0$) changes the radius of the reference sphere and can be used to compensate for spherical aberrations by relocating the location of minimal RMS spot size.

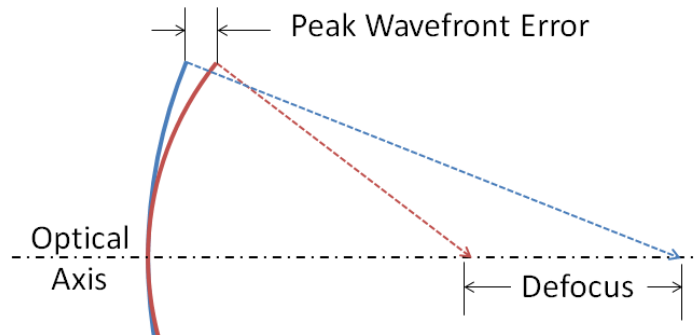


Figure 10: The reference sphere and ray (maroon) compared to the paraxial ray (blue). The diagram above shows an under corrected system.

1.4.2.2 Spherical Aberration: W_{040}

Spherical aberration occurs as a result of the marginal rays focusing to a different plane than the paraxial rays. Spherical aberration occurs uniformly across the field and can be reduced by bending the lens. Bending the lens involves adjusting the radii of the first and second surface to even out the power on each surface and therefore minimize the aberrations by having the second surface cancel out those introduced by the first surface¹⁰. The overall power of a lens system is maintained during the bending process.

Allowing the surface of the lens to be aspheric is another method for reducing spherical aberration, but comes at added manufacturing and inspection costs.

Splitting the lens into multiple elements creates additional surfaces allowing the individual surfaces to have lower powers, and thus contribute less to spherical aberration, while maintaining the system power. Splitting the lens increases the cost and complexity of the system and therefore is not considered an ideal option for this application.

Increasing the material index, allows the surface curvature or the element to decrease, thus reducing spherical aberration. For this application, higher index materials have lower transmission characteristics which are undesirable. The material with the most favorable index, transmission, and cost is Zinc Selenide. Lens materials will be discussed in greater detail in a subsequent section. (13)

¹⁰ In a positive meniscus lens the first and second surface have opposite powers due to the change in index (air to glass and then glass to air, for the first and second surface respectively).

Reducing the aperture size can also decrease spherical aberration (14). In this system the aperture size is the $1/e^2$ beam diameter and is constrained to a fixed value. Reducing the beam diameter would reduce the irradiance by increasing the diffraction limited spot size.

Spherical aberration can be balanced with defocus to minimize the spot size (8). The smallest spot size occurs where the marginal rays cross the caustic (after the marginal focus) the and is referred to as the minimum circle. The best Irradiance occurs at the smallest RMS spot size, which is generally located approximately 1/3 of the way between the paraxial and marginal focus (15).

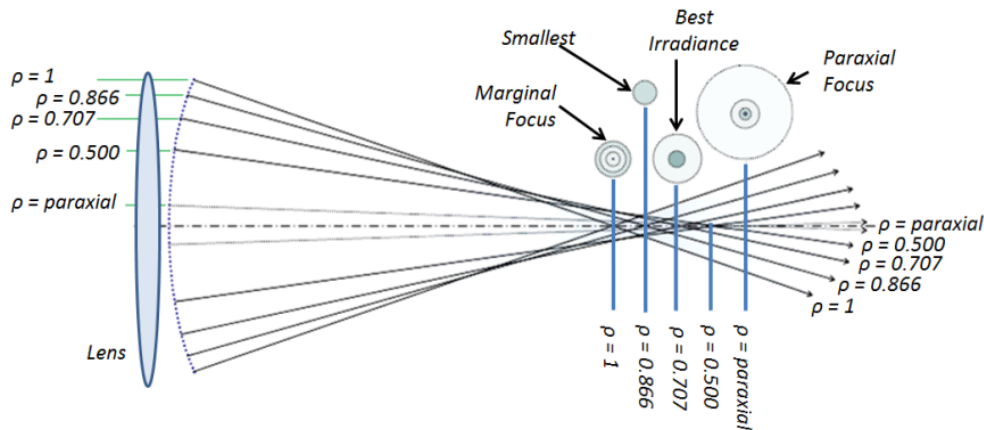


Figure 11: Spherical aberration and its effect on spot size. (9)

1.4.2.3 Coma Aberration: W131

Coma aberration occurs when different radial sections of the lens focus to a different plane than the paraxial rays. Coma can be reduced by appropriately bending a lens. The effects of bending the lens to reduce coma must be balanced against the reduction of other aberrations. (13)

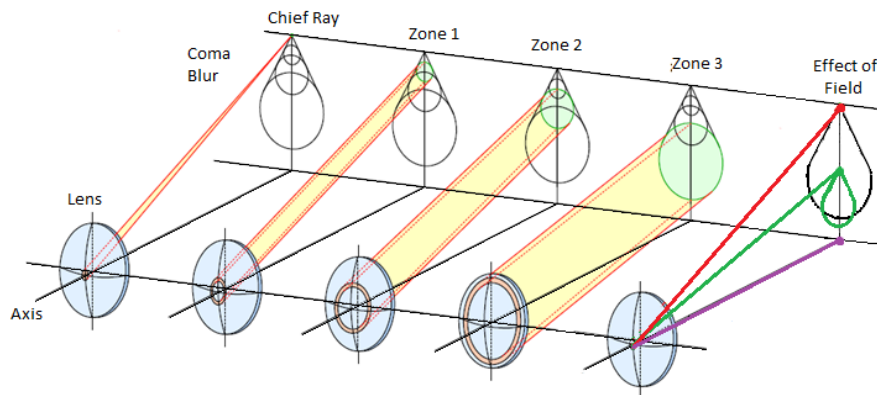


Figure 12: Coma occurs when the focal plane shifts with lens radius (Zones) and field of view. There is no Coma on axis. (16) The system to the far right shows how coma decreases with field position.

Coma can be minimized by placing the stop location as close as possible to the center of curvature of the first surface of the lens. However, it is not physically possible to have both the X and Y mirror locations at the center of curvature. Additionally, other system limitation such as the allowable diameter of the lens limits the spacing between the lens and the scanners. The distance midway between the 2 scanners was located as close as possible to the center of curvature of the first surface.

Allowing the surface of the lens to be aspheric is another method for reducing coma aberrations. This comes at added manufacturing and inspection costs.

Creating symmetry about the stop mitigates coma, as the aberrations introduced by the elements on one side of the stop cancel with the aberrations on the other side. Symmetry about the stop cannot be realized for this application.

1.4.2.4 Astigmatism Aberration: W222

Astigmatism is observed when the tangential and sagittal planes along a ray path focus at different locations. The difference varies across the field of view, and increases both with the power of the lens, and the incident ray angle. (14) The best focus in the presence of astigmatism occurs midway between the tangential and sagittal focal planes, where the ray caustics form a circle of least confusion.

To create a flat field, the circle of least confusion should ideally lie on a plane. Additionally, the size of the circle of least confusion can be minimized by decreasing the difference between the sagittal and tangential focus.

Allowing the surface of the lens to be aspheric is another method for reducing astigmatism aberrations. This comes at added manufacturing and inspection costs.

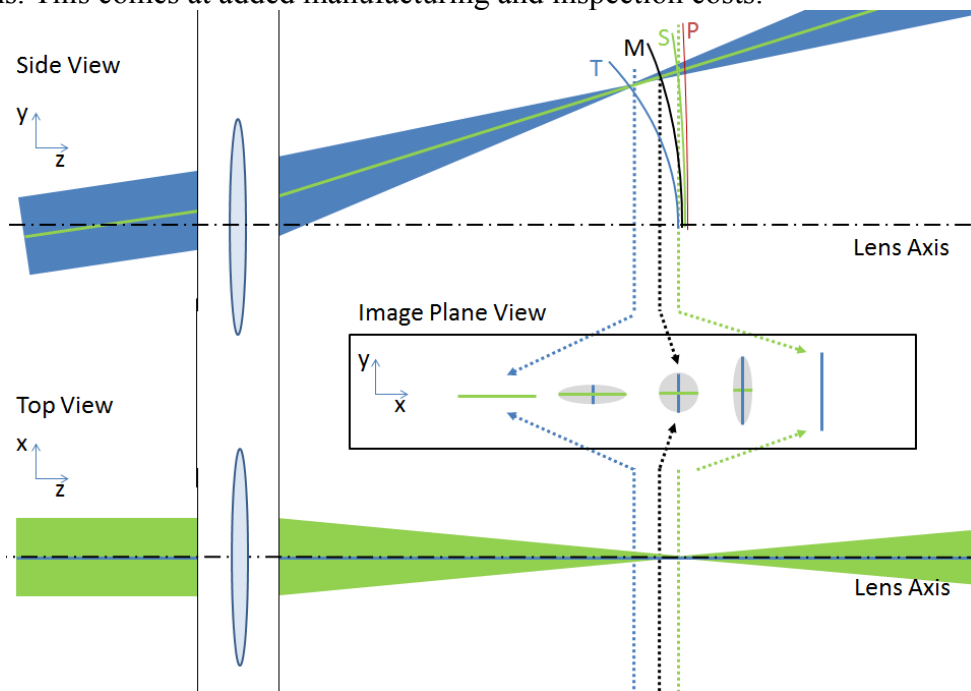


Figure 13: Astigmatism, and Field Curvature. Blue represents the rays in the tangential plane (T), green in the sagittal (S). The black line represents the medial (M) imaging surface where the smallest spot size is realized. The maroon line indicates the Petzval (P) surface. Dotted lines indicate the ideal focal location at the specific field of view shown; solid lines show the ideal focal location over the entire field of view (Side View Only). The Image Plane View shows what the spot diagram would like at the specific field of view.

1.4.2.5 Field Curvature Aberration: W_{220} and W_{220P}

Field curvature occurs because a spherical lens naturally focuses light to a spherical imaging surface. The natural field curvature created by the lens geometry and material properties results in the Petzval surface (W_{220P}). A positive lens creates an inward sloping curve (10). Decreasing the Petzval curvature creates a flatter imaging field.

For a scan lens the Petzval curvature can be evaluated with the following equation: (17)

$$c_{PS} = \frac{n_g - 1}{r_1 n_g} + \frac{1 - n_g}{r_2 n_g} = \frac{n_g - 1}{n_g} \left(\frac{1}{r_1} - \frac{1}{r_2} \right)$$

where:

c_{PS}	[mm ⁻¹]	Curvature of the Petzval surface, the radius would be: $r_{PS} = 1/c_{PS}$
n_g		Index of the scan lens glass
r_1	[mm]	Radius of curvature of the first surface, the curvature is: $c_1 = 1/r_1$
r_2	[mm]	Radius of curvature of the second surface, the curvature is: $c_2 = 1/r_2$

For a positive meniscus scan lens, both the radii are negative, and the index is a positive value greater than 1. To flatten the field a small curvature value can be realized as the value of r_1 approaches that of r_2 . Selecting a low index glass can also help flatten the field, however the selection of a lower index glass increases other aberrations.

The complete field curvature of the system (W_{220}) includes the incident ray data and the effect of astigmatism. Field curvature can be minimized by flattening the Petzval surface, and by introducing astigmatism to compensate for Petzval curvature.

1.4.2.6 Distortion Aberration: W_{311}

Distortion affects the location of the spot but not the wavefront error. A distortion free scan lens would meet the $f * \tan \theta$ with respect to the image height.

The Conventional scan lens described in this paper creates a distorted image. The distortion is a deviation from the $f * \tan \theta$ relationship. The Figure at right illustrates this observation.

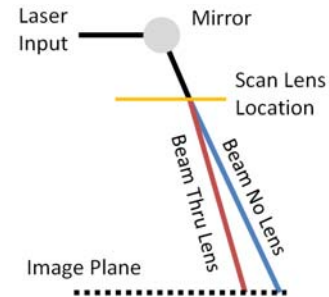


Figure 14: Simplified depiction of distortion in a Conventional scan lens.

The F-Theta Scan lens introduces distortion to create a linear relationship between the mirror deflection and the image height.

In addition to the distortion resulting from the optics, distortion will stem from the separation of the X and Y mirrors, which defines the object field of view. The separate X and Y mirrors act independently of each other with the resulting incident beam angle being a combination of the two mirror's deflection angles and not necessarily equal to either of them.

The type of distortion and severity is dependent on the type of scan lens. The F-Theta scan lens intentionally introduces a significant amount of distortion to create the linear $f * \theta$ relationship. Whereas a Conventional scan lens attempts to minimize the distortion. The distortion present in a Conventional scan lens typically results in cross between pincushion (sides of image, X at max angle) and barrel (top and bottom of image, Y at max angle) shape.

The distortion can be defined in terms of Polar or Cartesian coordinate systems. Polar coordinates provide a cleaner overview as radial distortion can be seen to increase with the distance from the center of the image and the tangential component is generally much smaller, and can often be ignored when developing correction equations. (18) (19) However, for the scan lens designed in this paper, the separate X and Y mirrors create more tangential distortion than a system with a single well defined stop. Additionally, because the X and Y mirror will be used to correct for the distortion it is beneficial to define the distortion in terms of its Cartesian X and Y components. The figure above shows pincushion distortion along with vectors indicating the radial, tangential, and Cartesian components.

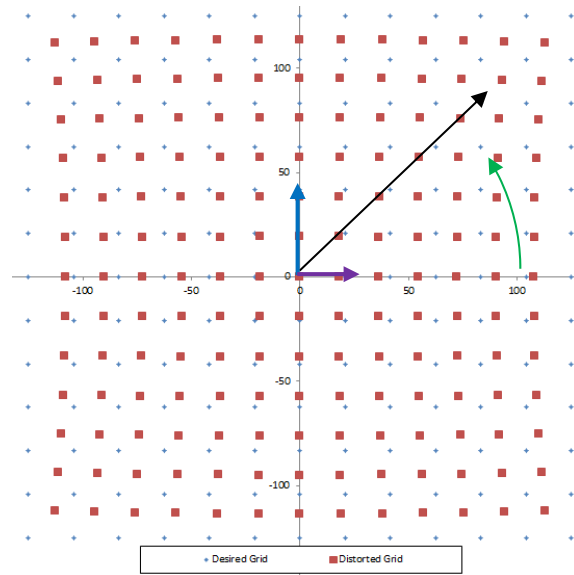


Figure 15: Example of Geometric Distortion over a 250x250mm. Polar: Green arrow indicates tangential, black arrow indicates radial distortion. Cartesian: Blue arrow indicates Y, purple arrow indicates X distortion. (directions shown are arbitrary)

The geometric distortion (location offset at each point) of a lens was modeled and a correction equation was developed to compensate for the distortion introduced by the lens. The compensation was applied to rotate the mirrors to an angle that effectively distorted the object to compensate for the optics and achieve a “distortion free” image. The correction equation was only developed for the Conventional scan lens system and will be reviewed in greater detail in a later section.

1.4.2.7 Other Aberrations

For completeness, aberrations not paramount to scan lens design are briefly reviewed in the table below:

Table 3: Aberration not relevant to scan lens design.	
Tilt or Magnification W_{111}	This characterizes the difference between the actual and paraxial (ideal) system magnification. Ray tracing accounts for tilt and magnification locating the spot in the magnified location on the image plane. The aberration is accounted for completely on the image plane and therefore the value is 0. Magnification was taken into consideration when developing the correction equation to account for the difference in location between the X and Y mirror.

Higher Order	The higher order term aberrations are not considered because their effect is small relative to the third order aberrations
Chromatic	The laser light is monochromatic and therefore chromatic aberrations do not need to be considered. ¹¹

¹¹ Many laser scanning systems include a “pointing laser” typical red (~630nm) to assist in system set-up and to demonstrate the location of the scanned image. This will not be considered in this report.

1.4.3 Evaluation of Aberrations

The prior discussion introduced aberrations and reviewed the methods available (within the allowable constraints of the marking system) to mitigate them. This section reviews how the magnitudes of the aberrations were determined along with how the system was configured to optimize performance.

The ensuing discussion pertains to the evaluation of a Conventional single element scan lens. Additional lenses could be added (if needed) to the system but they would complicate the analysis by providing more degrees of freedom without providing additional insight to the principles of aberration mitigation.

The Conventional scan lens was assumed to be a single element thick lens located a fixed distance from the stop. The system aberrations were quantified using the Seidel coefficients which are derived from the physical lens geometry, material, and stop location along with the data accumulated by tracing rays through the system (see Appendix 2 for equations). (20) (7)The system is shown in the Figure below.

The thickness of the lens, as well as, its location relative to the stop can be varied. To decrease coma the stop should be located as close as possible to the center of curvature of the surfaces, which in this case places the lens at the maximum allowable distance¹². Likewise, to decrease the surface power of the lens, and thus decrease spherical, coma, and astigmatism, the lens thickness of the glass should be at the maximum.

The radii are also variable and the lens can be subjected to bending. To evaluate the effect of bending the lens on system aberrations, the overall system power was approximated¹³ and rays were traced through individual systems with different lens shape factors. The meniscus lens was oriented so the concave surface was the first surface to minimize aberrations by balancing the surface powers. Both

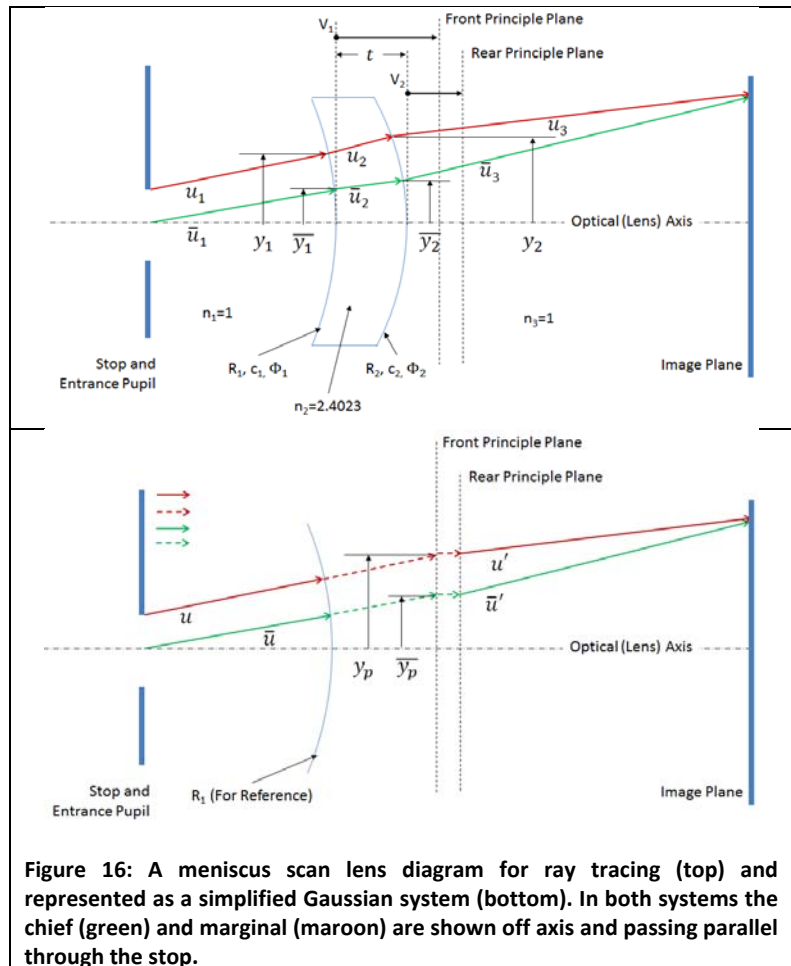


Figure 16: A meniscus scan lens diagram for ray tracing (top) and represented as a simplified Gaussian system (bottom). In both systems the chief (green) and marginal (maroon) are shown off axis and passing parallel through the stop.

¹² the power of the first surface required a radius greater than the allowable thickness

¹³ System power was estimated based on the defined object field of view and image height requirement

surfaces have similar negative radii, but due to the change in index, their powers have opposite signs therefore the aberrations created by the power of the first surface partially, or completely, cancel the aberrations created by the power of the second surface.

The chief and marginal rays were oriented to the maximum object field of view which is the worst case orientation for aberrations. The results of the analysis are shown below.

Lens Bending Effect on Total Aberrations (Image Corner)

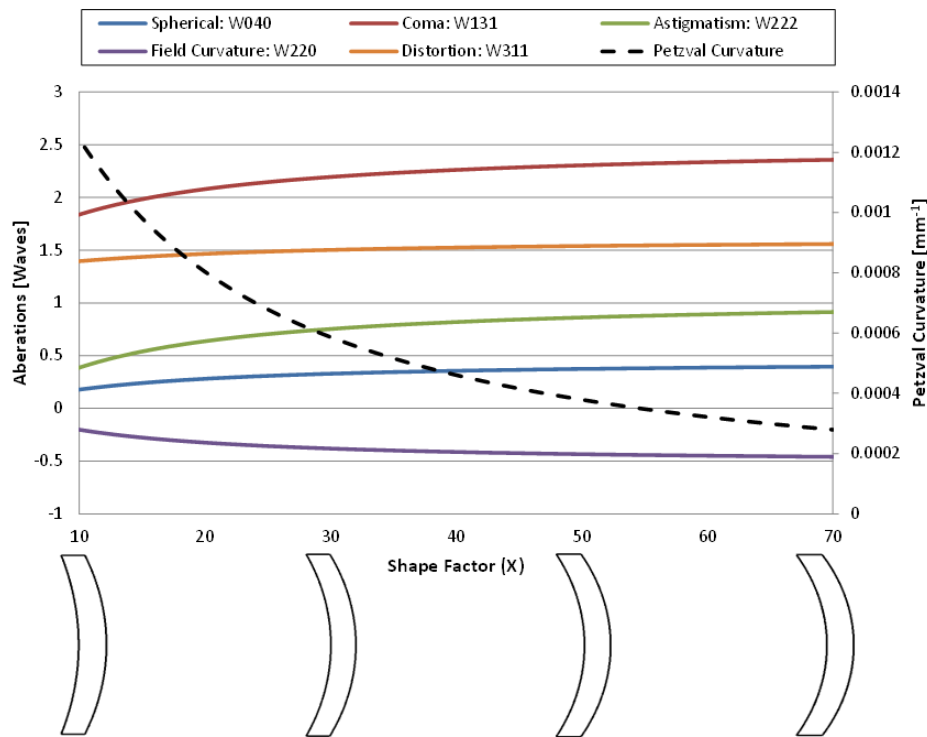


Figure 17: The effect of bending the lens on total system aberrations at the maximum object field of view (the curvature of both surfaces increase from left to right)

The results indicated that coma would dominate, which was expected due to the large field of view and asymmetry about the stop. Astigmatism and field curvature have opposite signs and a similar magnitude due to their dependence on pupil coordinate and field height, and therefore would partially cancel out (in some orientations more so than others due to the azimuthal angle dependence of astigmatism). The spherical aberration could be compensated by introducing defocus.

The results also show that Petzval field curvature is minimized with shape factors that increase the magnitude of the other aberrations. This illustrates why it is necessary to allow some aberrations in order to achieve a flat field. The goal then becomes to cancel out the aberrations that are allowed to minimize their effect. The balancing of aberrations between surfaces is illustrated in the figure below which shows the effect of lens bending on aberrations for each

surface in the system. Notice the slopes of the aberration curves have opposite signs on opposite powered surfaces.

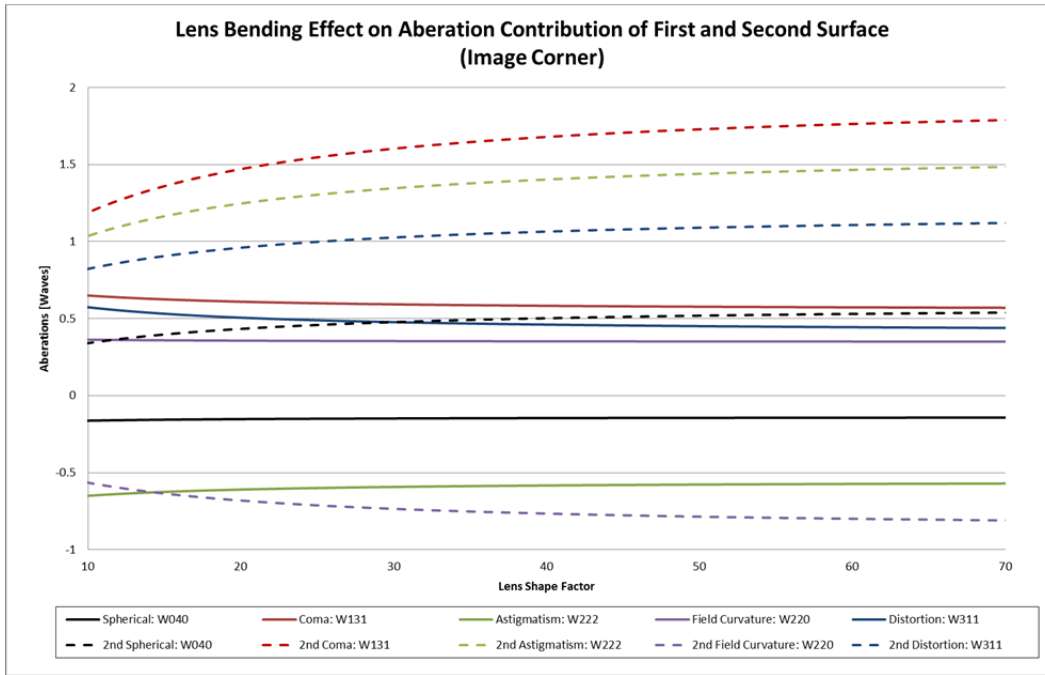


Figure 18: The effect of bending the lens and the aberrations introduced at each surface. Solid lines denote first surface, dotted lines denote second surface.

1.4.4 Lens Coating

Lens coatings are used to enhance optical properties. The systems described in this thesis required high overall system transmittance efficiency and so to facilitate the transfer of light through the system an anti-reflective (AR) coating was applied to all glass surfaces in the Zemax model. AR coatings are designed to minimize reflection, and maximize the transmission of light from one medium to the next by adding additional layers to the interface between mediums (in this case air to glass, and glass to air). Any light that does reflect from one interface should destructively interfere with the reflected light from a subsequent interface, effectively cancelling each other out.

The layers of the AR coating are thin films typically applied by vapor deposition. The effectiveness of the coating is dependent on the thickness, number, and refractive index of the layers along with the orientation relative to the incident beam. The thickness and index of refraction are wavelength dependent parameters; therefore AR coatings are only effective for specific wavelengths (and/or wavelength ranges). Typically, the AR coating can be made more efficient as the range of wavelengths (bandwidth) becomes narrower.

Lens coating designed to be more durable (resist scratching, etc.) are also available, and would benefit the longevity for the scan lens. The drawback to durable coatings is poor transmittance relative to AR coatings, and therefore a durable coating was not used for this scan lens design.

1.4.5 Lens Material

The common lens materials for long wave infrared scan lenses include Zinc Selenide (ZnSe), Gallium Arsenide (GaAs), and Germanium (Ge). Germanium has the highest index of refraction but is difficult to mine and process resulting in higher costs despite requiring less material due to the higher index but it also has the lowest transmission rate. Gallium Arsenide is the hardest (best wear characteristics), but less transparent than Zinc Selenide reducing the overall power throughput. A summary of the pertinent material properties are listed in the Table below.

Property ¹⁴	Units	ZnSe	Ge	GaAs
Refractive Index		2.4295	4.004	3.2701
Transmission ¹⁵	[%]	72	46	57
Bulk Absorption Coefficient	[1/cm]	< 0.24	<0.03	<0.01
Temp. Change of Refractive Index	[1/C]	41x10 ⁻⁶	408x10 ⁻⁶	149x10 ⁻⁶
Thermal Conductivity	[W/cm-C]	0.18	0.59	0.48
Specific Heat	[J/g-C]	0.356	0.31	0.325
Linear Expansion Coefficient	[1/C]	7.57x10 ⁻⁶	5.7x10 ⁻⁶	5.7x10 ⁻⁶
Young 's Modulus	[GPa]	67.2	100	83
Knoop Hardness	[Kg/mm ²]	105-120	692	750
Density	[g/cm ³]	5.27	5.32	5.37
Rupture Hardness	[MPa]	55.1	93	138

Zinc Selenide offered more favorable properties than the other glasses for the application described in this thesis and therefore was the glass selected for the scan lens design.

Zinc Selenide is a crystal grown at high temperatures using vapor deposition of a gaseous mixture of Zinc and Selenide. The material is part of the II-VI grouping of semi conductive materials (Zinc 2nd column of the periodic table, and Selenide is from the 6th). The blank is typically grown in a 1 meter diameter slab ~12mm thick (this allows for ~10mm of useable lens thickness). Optical blanks are then cut from the large crystal and sorted by thickness. The final lens is generally produced by diamond turning the blank. The diamond turning process is precise enough so no grinding or polishing is necessary.

The two largest manufacturers of ZnSe are II-VI and Dow (Ophir is the preferred customer of Dow).

1.4.6 Correction Equation Development Overview

The Conventional scan lens design contained distortion. The distortion was compensated for by developing correction equations that adjust the X and Y mirror tilt angles (effectively distorting the object) to produce a non-distorted image. The adjustment to the scan angle needed to be transparent to the end user, i.e. the end user was able to create a non-distorted image in the user

¹⁴ All properties listed for 10.6 μm and 20 C.

¹⁵ Transmission for ~2mm thickness (27) this can be increased with Anti-Reflective (AR) coatings

interface of the marking system software and have that image appear undistorted on the substrate that was marked.

The correction equation was applied to the scanning mirror orientation, therefore the equation solved for a mechanical angle. The approach taken to derive the distortion correction equation is described in this section.

A model of the optical system was created in Zemax. The model included the laser source, scanning mirrors, an optimized scan lens, and the image plane. A macro was used to create a checkerboard pattern on the image plane (Step 1) and then calculate the X and Y scan angle for each node in the pattern (Step 2) based on the mirror deflection angles and the locations of the scanners relative to the image plane. The effects of the optics were not considered during the calculation of the angle. A pinhole imaging approximation was assumed. (19)

The mirror tilts for each configuration were input to the Zemax model and rays were traced through the system and their location on the image plane was recorded. (Step 3) This was done for each configuration (node in the checkerboard) (Step 4).

The difference in location between the ideal and distorted nodes was evaluated and reduced to separable X and Y distance errors (Step 5). The X and Y distance errors were converted to X and Y angle errors using the approach taken in Step 2 but with an added magnification factor. This was done for each location. The result was a file containing the X and Y angular distortion at each node on the image plane (Step 6).

The angular distortion files were imported into Matlab, and best fit polynomials were created to characterize the X and Y distortion with the cftool functionality using a linear least square fit algorithm.

The X and Y distortion correction polynomials were input to the macro. The macro applied the correction equations to the angles calculated in Step 2. Rays were retraced through the system for each configuration (Step 3*) and the corrected checkerboard pattern was created (Step 4*). The corrected checkerboard pattern was compared to the ideal checkerboard pattern to validate the accuracy of the correction equations (Step 5*).

An overview of the approach is shown in the Figure on the next page.

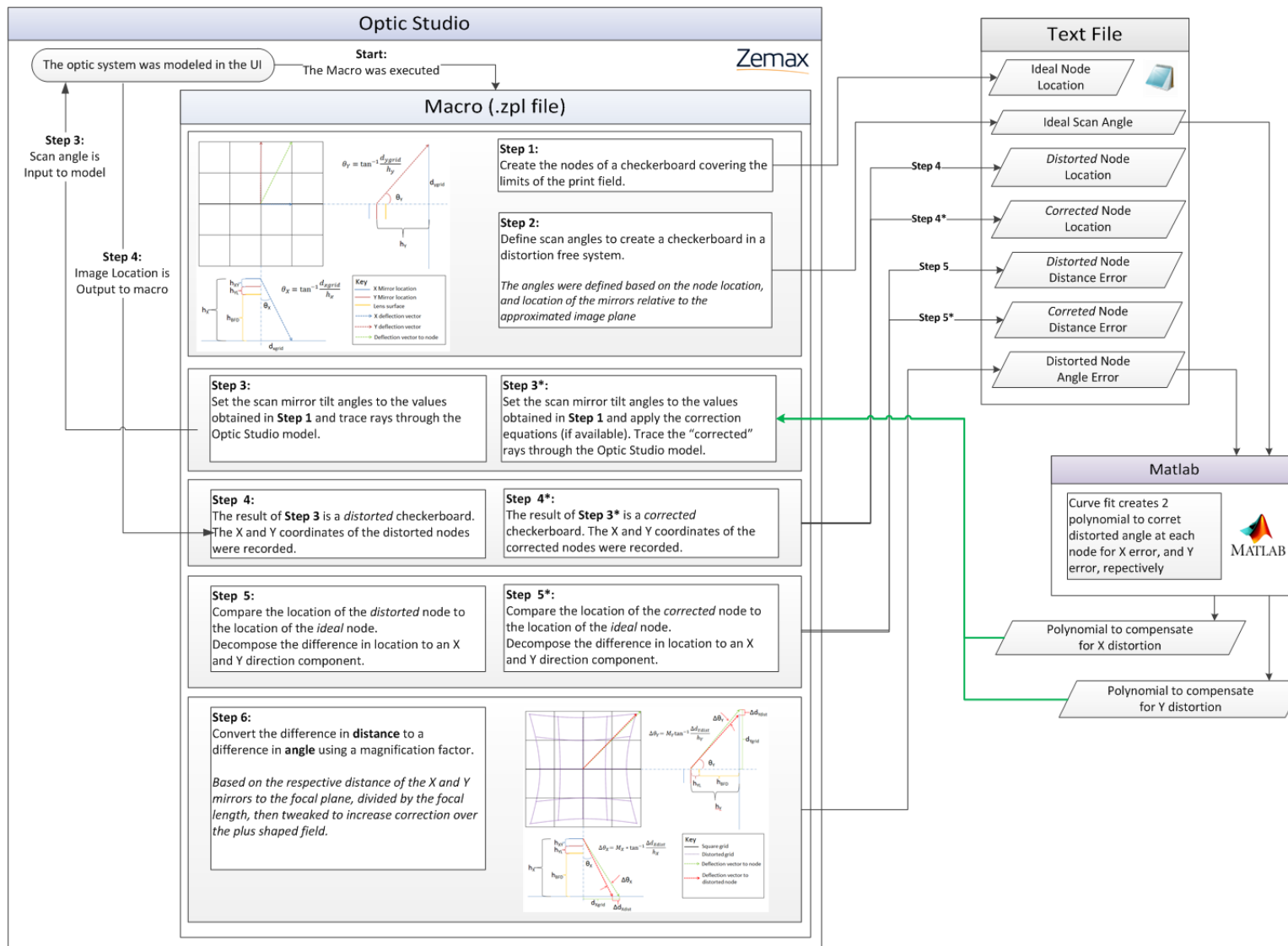


Figure 19: Correction Equation development flow chart.

2. Scan Lens Design

This section describes the scan lens design process. The process started by defining the known constraints, requirements, assumptions and limitations. Various systems were then designed, optimized and evaluated based on the requirement metrics. The designs involved creating models of increasing complexity.

The first model was a symmetric (about the optical axis) system with a fixed stop location used to define the field of view. This system will be referred to as the *Simplified System*. The rotationally symmetric design allowed the evaluation and mitigation of the aberrations previously discussed and along with the full use of the design and evaluation tools supplied by Zemax. The *Simplified System* allowed distortion and no attempt was made to correlate or evaluate the spot location relative to the field of view. The geometry of the optimized *Simplified System* served as a baseline for the more complex systems.

Building on the *Simplified System* a non-symmetric, 2 mirror *Scanning System* was designed and optimized in Zemax. The *Scanning System* made use of the mirrors' tilt angles to define the object field of view. Each pair of tilt angles represented a unique configuration. The design was optimized for a single field in multiple configurations as opposed to the multiple fields in a single configuration used for the *Simplified System* design. No attempt was made to correct the distortion; however the distortion was evaluated over the field with a macro and used to create distortion correction equations with Matlab. The distortion correction equations were then input to the optic system with a macro and the accuracy of the corrected image was evaluated.

The *Scanning System* was then allowed to have an aspheric surface to determine if any performance gains could be realized. This system will be referred to as the *Aspheric Scanning System*. The *Aspheric Scanning System* was optimized and evaluated in the same way as the *Scanning System*.

The *Simplified System* was then optimized to meet to meet the F-theta criteria. A single element system proved incapable of meeting the F-Theta criteria without significantly compromising the other performance metrics due to the large field size. A second lens was introduced to the *Simplified System* creating a new system that will be referred to as the *F-Theta Simplified System*. This 2 element system was optimized to meet the F-Theta distortion condition.

Using the geometry of the *F-Theta Simplified System* a 2 element non-symmetric *F-Theta Scanning System* was modeled. This system was then optimized to meet the F-Theta criteria in the Y-axis. A summary of the system is listed in the table below and shown visually in the figure on the next page.

System	<i>Simplified System</i>	<i>Scanning System</i>	<i>Aspheric Scanning System</i>	<i>F-Theta Simplified System</i>	<i>F-Theta Scanning System</i>
Number of Elements	1	1	1	2	2
Symmetry about Optic Axis	Yes	No	No	Yes	No
Field of View	Defined by Fields at Stop	Defined by Mirror Tilt	Defined by Mirror Tilt	Defined by Fields at Stop	Defined by Mirror Tilt
Surfaces	Spherical	Spherical	Spherical & Aspheric	Spherical	Spherical
Distortion	No Consideration	Corrected with Equation	Corrected with Equation	F-Theta Criteria	F-Theta Criteria

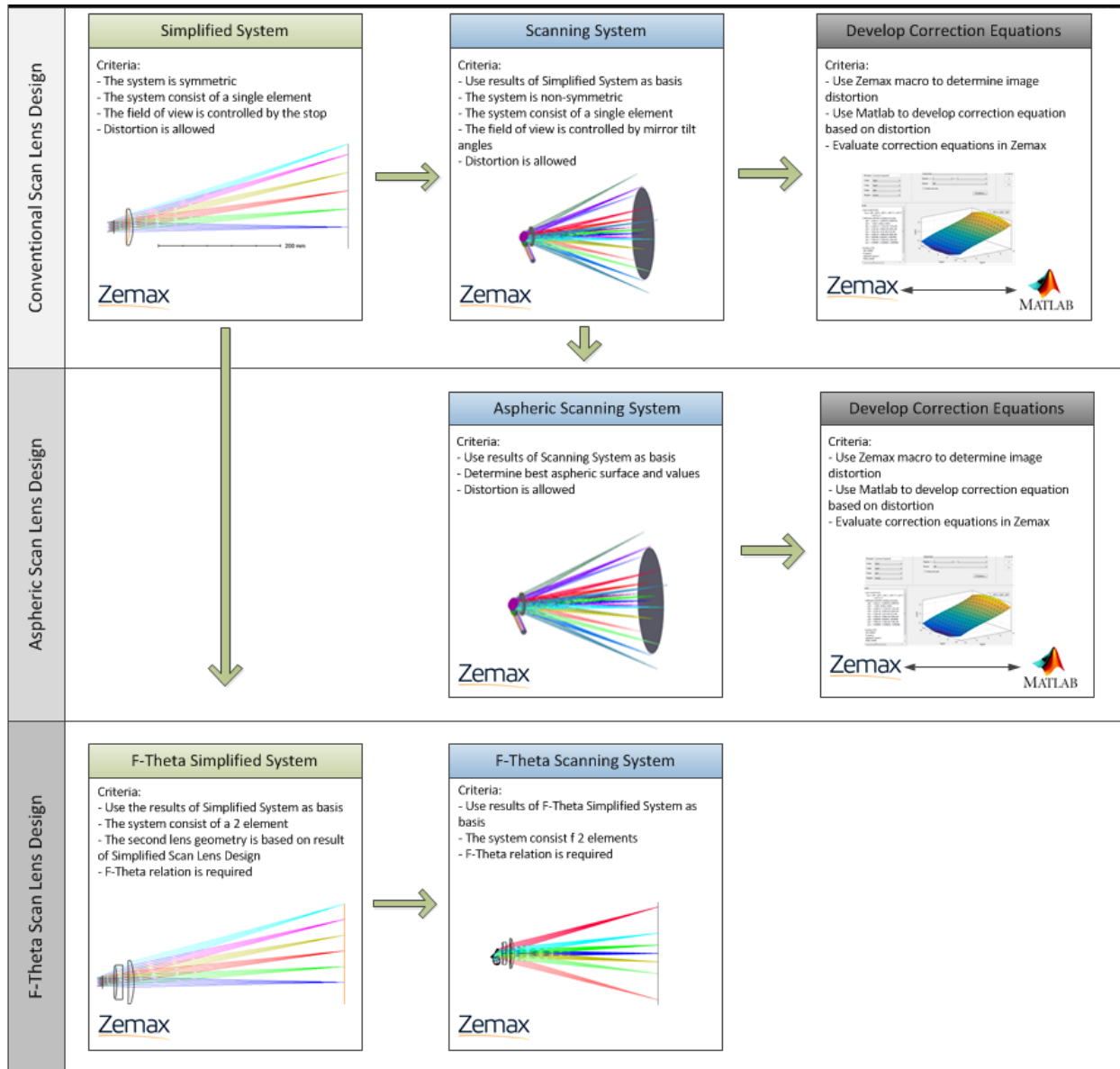


Figure 20: Overview of the Systems designed and their progression.

2.1 Constraints and Requirements

The system constraints and requirements presented in the table below are applicable to all systems.

Table 6: Scan lens requirements, and constraints for all systems.	
Scanner Constraints	
The X and Y scanner will have +/-11° mechanical rotation (+/-22° Optical).	
The distance from the Y mirror mount to the lens mounting surface should be between 17.477mm to 20.477mm	
The distance between the scan mirrors is fixed at 19.24mm (when mirrors are in their nominal location)	
Laser Constraints	
The object is a collimated laser beam with $1/e^2$ diameter of 14mm	
The wavelength is 10.6 μm	
The irradiance profile is Gaussian TEM ₀₀ ($M^2 = 1$)	
The laser output power was 40W continuous wave (CW)	
Print Field Requirements	
The print field must cover a plus shaped field (intersection of vertical and horizontal rectangles with dimensions of 250x110mm = 273mm diagonal)	
The correction equation should locate spots within an accuracy of 1% of the minimum image dimension (within 1.10 mm).	
The F-Theta lens should be accurate to within 1% of the criteria for a single axis	
Spot (Image of Laser Beam) Requirements	
Spots on within the print field should be within 5% of the diffraction limit	
The peak irradiance should be maximized, and balanced against irradiance uniformity across the print field.	
The RMS spot size should be minimized to maximize irradiance across the field.	

The physical requirements pertaining to the lens design are unique to the system. The values are presented in the table below:

Table 7: Physical lens requirements¹⁶					
	<i>Simplified System</i>	<i>Scanning System</i>	<i>Aspheric Scanning System</i>	<i>F-Theta Simplified System</i>	<i>F-Theta Scanning System</i>
# Elements		1		2	
Lens Diameter		60		80	
Clear Aperture		57		75	
Center Thickness		5.0 to 10.0			
Edge Thickness		3.50 to 5.50		3.50 to 15.0	
Radii		Spherical	Aspheric	Spherical	
Material		ZnSe			

The system should also be designed to minimize cost. Aspheric surfaces and the additional elements necessary for an F-Theta lens incur added cost. The more expensive solutions were still

¹⁶ All dimensions in mm unless otherwise stated

evaluated to understand what the performance to cost ratio was and therefore allow an educated decision to be made concerning if the added cost was warranted.

Tunnel diagrams of systems are shown in the Figure below:

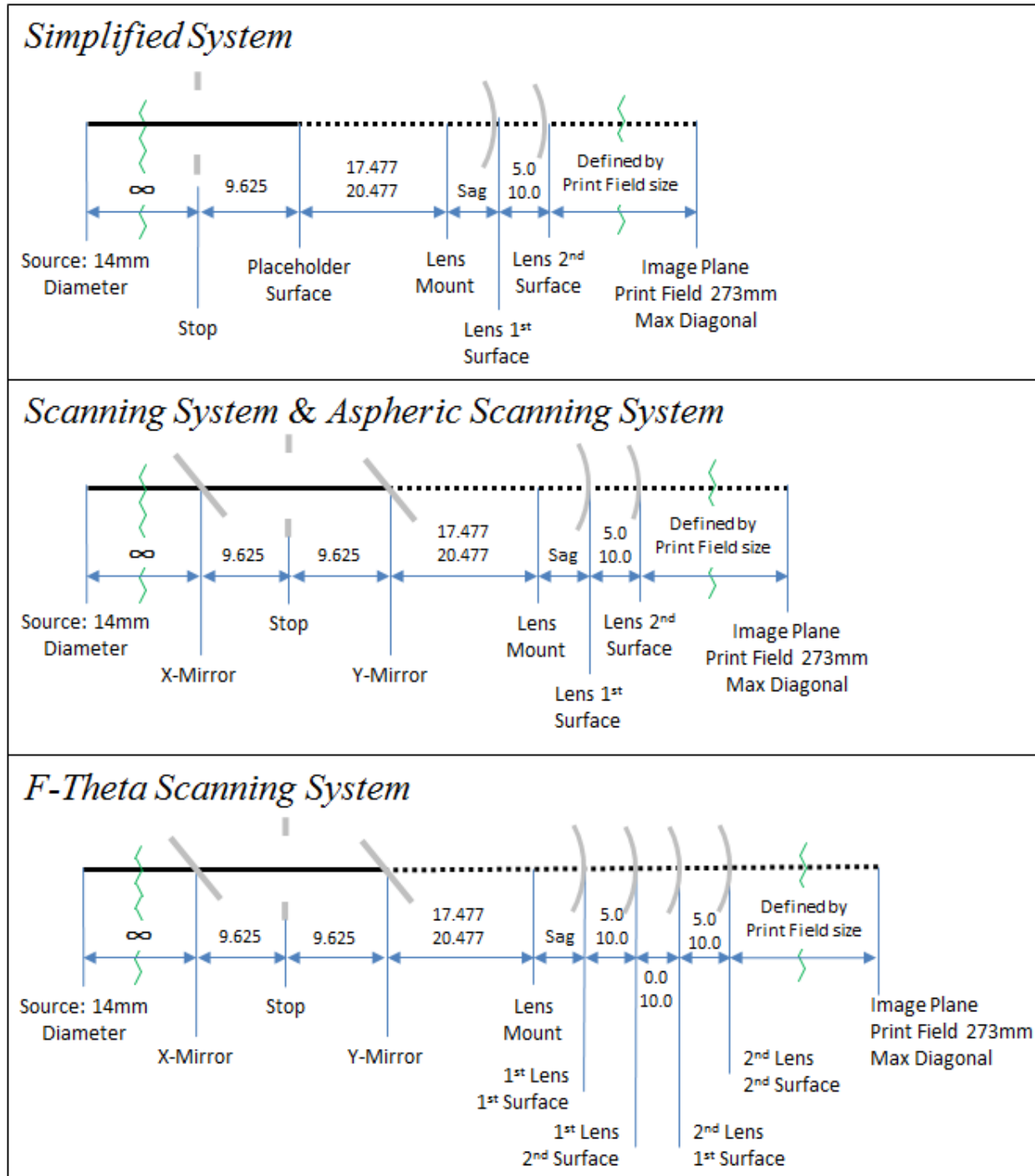


Figure 21: Tunnel diagram of scan lens design parameters¹⁷ (solid black line denotes the beam path, dotted line represents a length of the beam path can be used as an optimization parameter).

¹⁷ All dimensions in mm unless otherwise stated

2.2 Image Quality

The image quality was evaluated by the following metrics, in order of importance:

2.2.1 Print Field

The application required a “+” shaped print field with dimension of 250x110mm defining the horizontal and vertical rectangles. The figure to the right shows the print field geometry along with a visual depiction of the projected scan lens and scan mirror pupils (not to scale) on the print field plane.

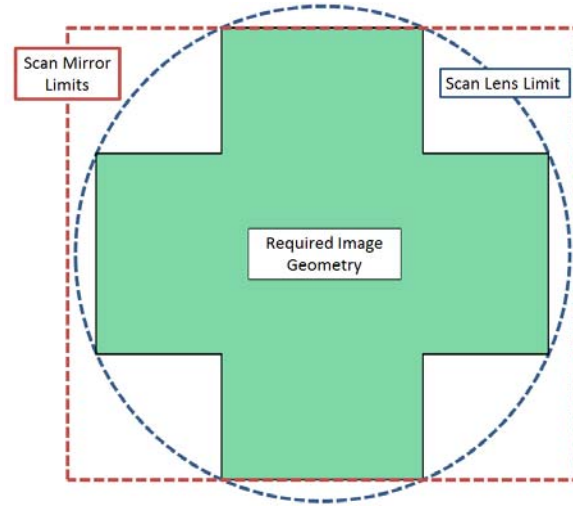


Figure 22: Print field size and shape requirements.

The print field geometry was not to be limited by any of the system apertures. The location of the spot at the corners of the print field was determined using the coordinates of the spot centroid (in Zemax: CENY, and CENX was used to evaluate all spot location in the macro). This was also validated from the coordinates included on the spot diagram created from the Zemax User Interface (for a single Field and Configuration).

2.2.2 Irradiance: Peak and Uniformity

High peak irradiance was desired and achieved by minimizing the RMS spot size and creating a nearly diffraction limited design over the entire print field at the shortest possible focal length. The irradiance of a diffraction limited image in a scanning system is proportional to the incident power and inversely related to area of the focused spot. (22)

$$I_{Peak} = \frac{2P}{\pi \left(\frac{D_{Spot}}{2}\right)^2} = \frac{\pi P}{2M^2} \left(\frac{D_{beam}}{\lambda f}\right)^2$$

where:

I_{Peak}	[W/mm]	Peak irradiance at the center of the spot	----
P	[W]	Power of laser	Fixed = 40 W
D_{Spot}	[μm]	The diameter of the focused image spot	----
D_{beam}	[mm]	The diameter ($1/e^2$) of the incident beam at the lens	Fixed = 14 mm
M^2		The quality of the incident beam (<1.2 is typical)	Fixed = 1.0
λ	[μm]	The wavelength of the incident beam	Fixed = 10.6 μm
f	[mm]	The focal length	Variable

The focal length is the only variable available for the optimization of this system. From the equation above it can be seen that a small value of f (a shorter focal length) will result in a higher irradiance value. Furthermore, the Irradiance is dependent on the square of the F-number, which in the case of the scanning system with a fixed beam diameter reduces to the square of the focal length, magnifying the effect. Therefore to maximize the irradiance the shortest possible focal length that allows the field size to be achieved was selected. The short focal length came at the expense of irradiance uniformity across the print field and depth of focus. The irradiance calculation above does not take into consideration limiting apertures or aberration effects.

The uniformity of the irradiance across the print field will be evaluated by comparing the peak irradiance of a spot at the print field center to the peak irradiance of a spot at the print field corner. The peak intensity at the corner of the print field will be reduced due to aberrations and a non-orthogonal incident angle of the beam to the image surface. The effect of the non-orthogonal incident beam on the spot irradiance is shown below.

$$I_{Dev} \sim \frac{I_{Corner}}{I_{Center}} \sim \frac{A_{Corner}}{A_{Center}}$$

where:

I_{Dev}	[%]	Irradiance deviation across the print field
I_{Corner}	[W/mm]	Peak irradiance of a spot at the corner of the print field
I_{Center}	[W/mm]	Peak irradiance a spot at the center of the print field
A_{Corner}	[mm]	The area of the spot at the corner of the print field, projected onto the image plane
A_{Center}	[μ m]	The area of the spot at the center of the print field

Spot Diagrams were used to evaluate the spot size defined by the ray footprint and the Airy disk. The ray footprint shows the transverse spread of the ray bundles incident on the image plane and is purely a construct of the ray tracing without consideration of diffraction. The ray footprint can be used to determine aberrations based on the shape and ray density distribution.

The Airy disk is the diameter of the first null in an Airy diffraction pattern and represents the smallest spot size allowed by the effects of diffraction. The system cannot produce a smaller spot even if the spot footprint predicted by the ray trace is much smaller than the Airy disc. The spot diagram overlaid with the Airy disc was a coarse estimate to determine if the design was near the diffraction limit. (22)

Physical Optics Propagation (POP) of a beam through the system was used to evaluate the magnitude of the peak irradiance of the spots at both the center and corner of the print field. POP includes the effect of limiting apertures on the beam propagation and the resulting diffraction (loss of irradiance) that occurs. The irradiance was measured normal to the image plane.

Huygens Diffraction Encircled Energy Plots were plotted for imaged spots at both the center and corner of the print field to determine how close the design was to the diffraction limit at those locations.

Huygens Point Spread Function (PSF) cross sections of the imaged spots were created both at the center and corner of the print field (both the X and Y beam profiles of the imaged spot were plotted at the print field corners due to the non-orthogonal incidence). The Huygens PSF cross sections were oriented normal to the image plane, and show the normalized irradiance of the imaged spots at both the center and corner of the print field.

2.2.3 Distortion

The distortion introduced by the lens was modeled and evaluated for all systems that included scan mirrors. The distortion of the *Scanning System* and *Aspheric Scanning System* was evaluated after the application of the correction equations. The corrected image was required to be within 1% of the minimum image dimension (110mm) which correlates to 1.1 mm. This value is acceptable given the application of the system.

The F-Theta lens image accuracy was required to be within 1% (1.1mm) of the image defined by the namesake's criteria, no correction equations were applied.

2.3 Assumptions and Limitations

The following assumptions (not already listed elsewhere) were made during the design and optimization of the systems highlighted in this Thesis:

- All component values were nominal and tolerances (manufacturing or assembly) were not considered.
- The offset from the mirror surface to the rotational axis of the scanner was not considered
- Generic AR coatings were used in the Zemax model
- The mirror profile was estimated using ellipses rather than the actual profile
- Laser polarization was not considered in the irradiance calculations (the polarization affects the reflectivity of mirrors)
- The angular dependence of the mirror reflectivity was not considered in the irradiance calculations
- The marking system imaging algorithm is not based on continuous scanning motion.

2.4 Modeling the Systems

The systems were modeled in Zemax Optic Studio Professional Release 16. All models included a collimated 14mm diameter beam with Gaussian apodization at 10.6 μm . The field of view was defined, either as multiple fields at different angles or as multiple configuration controlling the scan mirrors tilt angles. Values for the lens radii and thickness were inserted to loosely approximate what the expected system would be. The default AR coating was applied to all lens surfaces.

A merit function was defined to optimize the system based on the information presented in the **Constraints and Requirements** section. Thicknesses between surfaces were constrained by the following operands: MNCA, MXCA, MCG, MXCG, for air and glass mediums respectively. The edge thickness of the lens was confined with the MNEG, and MXEG operands. A Default Merit Function (DMFS) was used to minimize the RMS Spot Radius with respect to the Centroid over the image plane using the TRAC operand. Distortion was evaluated, and in some cases constrained using the CENX and CENY operands.

The systems were then optimized using the *Local Optimization* functionality. The optimization was done iteratively, and the model was updated as necessary to reflect changes in focal length, field size, lens sag, and lens thickness. After completing the *Local Optimization*, a *Global Optimization* of over 2 million systems was executed to ensure the optimized system was not a local minimum. The *Quick Focus* tool was used after each optimization to define the image plane for the system based on the minimal spot radius with respect to the centroid.

The image quality of the final designs was evaluated with the metrics defined in the **Image Quality** section. The five systems previously mentioned were modeled. More detail related to the specific models is presented in the following sections.

2.4.1 Simplified System

The first model analyzed was a *Simplified System* with no scan mirrors. This model was axially symmetric (2D). The stop was fixed at a location half-way between where the scan mirrors would be. The field of view was defined in terms of the image height at intervals of 0, 30, 60, 90,

120, and 137mm. The system was then optimized over all 6 fields using the optimization process previously described. The layout appeared similar to the Figure below.

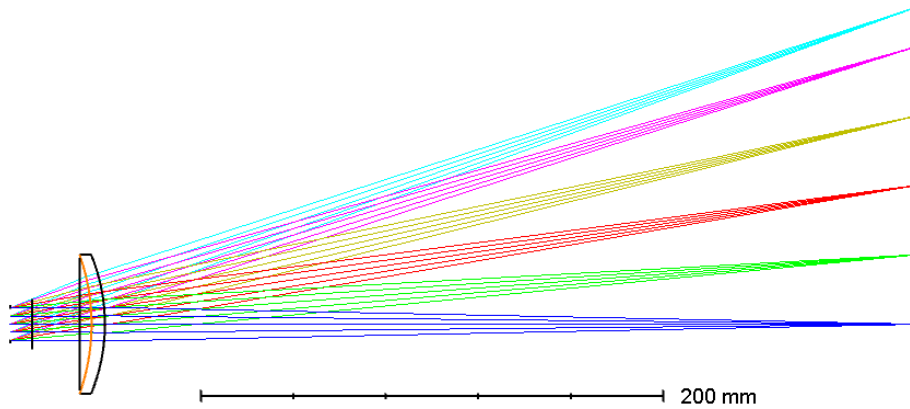


Figure 23: Layout for the *Simplified System*. Fields are represented by different colored ray bundles.

The intent of this model was twofold. This model is a simplified version of the actual system and as such it is easier to set up, manipulate, and evaluate making it useful in determining the approximate settings and values that can be used as a baseline for the more complex systems. The performance of this model was compared against the performance of the *Scanning System* model to determine if the extra effort to create the *Scanning System* model was warranted. Due to the simplified nature of this model distortion correction equations were not developed.

2.4.1.1 Results

The optimized system attributes are presented in the table below.

Table 8: Optimal geometry for the *Simplified System*

Simplified System Geometry						
Laser	Stop	Placeholder Surface	Lens Mount	First Surface	Second Surface	Image
Thickness [mm]:	∞	9.625	20.477	5.35	5.867	336.863
Radius [mm]:	∞	∞	∞	-72.289	-65.318	∞
Semi Diameter [mm] :	7	n/a	28.5	30	30	137
Focal Length [mm]:	n/a	n/a	n/a	n/a	323.8	n/a
Lens Power [mm^{-1}]:	n/a	n/a	n/a	n/a	0.00309	n/a
Edge Thickness [mm]:	n/a	n/a	n/a	n/a	5.09	n/a

The total system aberrations in terms of waves are summarized in the table below.

Table 9: Sum of Aberrations in the *Simplified System* at the image

Spherical	Coma	Astigmatism	Petzval Field Curvature	Distortion	Defocus	Tilt / Magnification
W040	W131	W222	W220P	W311	W020	W111
0.0336	-0.0989	-0.0937	0.1718	4.7786	0	0

The aberration contribution of each surface in the system is shown in the Figure below.

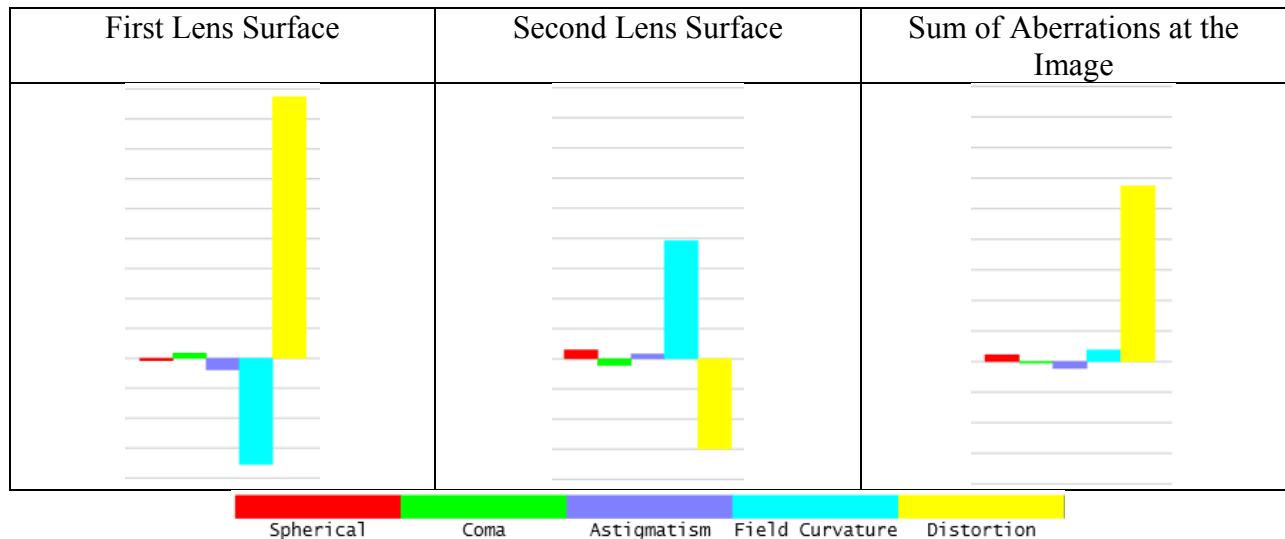


Figure 24: Aberrations as each surface of the *Simplified System* Scale is 20 μ m / horizontal bar. The max total distortion is ~0.1 mm

The field curvature and distortion are the dominant system aberrations at each surface. However, bending of the lens has resulted in balancing the aberration created by the first and second surface (the field curvature, spherical, coma, and astigmatism aberrations are nearly cancelled). The small amount of total astigmatism, nearly balances that of field curvature. The total system distortion is significantly larger than the other aberrations, but this doesn't affect the spot quality.

The image quality, as measured by the diffraction encircled energy, at both the center and edge of the print field are shown in the figure below.

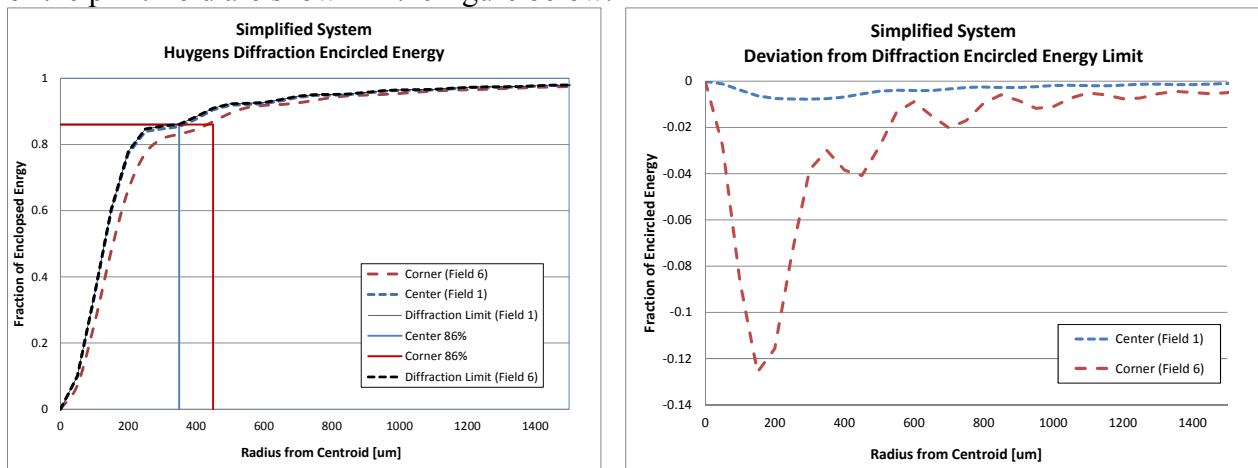


Figure 25: Diffraction encircled energy of the *Simplified System* compared to the diffraction limit. The system is within 1% at the print field center and 13% at the print field corner

The plot to the right shows just the difference between the predicted system performance and the diffraction limit. The encircled energy at both the center and corner of the print field is within 13% of the diffraction limit which does not meet the requirements.

The Huygens PSF takes diffraction into consideration, with respect to the ray path, when determining the spot irradiance profile. Loss of irradiance due to apertures (as long as the ray

passes through) is not accounted for. The profile shown has a normalized irradiance of 1 located at the print field center. The maximum irradiance at the corner of the print field is approximately 17% less than at the center (correlating well with the prediction of the diffraction enclosed energy plots). The cross section of the Huygens PSF, shown in the Figure below includes the predicted diffraction limited spot size (314 μ m). All cross sections show irradiance normal to the image surface.

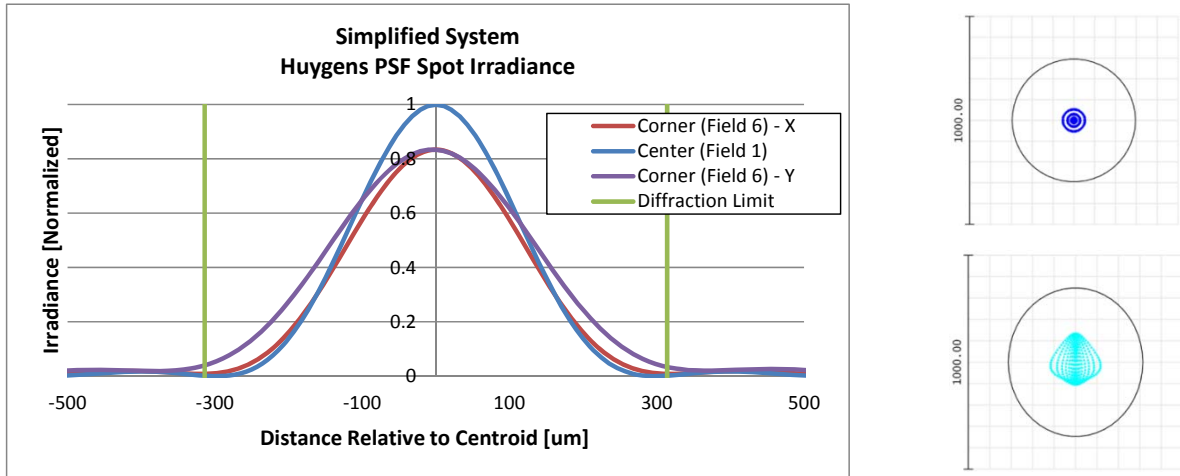


Figure 26: Huygens PSF Spot Irradiance of the *Simplified System* (left), spot diagrams displayed with the Airy disk at the image center (top right), and corner (bottom right)

The spot diagrams and the resulting radii of the ray bundles as they appear on the image plane are well within the Airy disk. The spot shapes are useful in illustrating the astigmatism in the corner of the print field, but measuring the radii of the ray bundles is not an accurate assessment of the spot size. To obtain an accurate spot size the effects of diffraction must be included.

Physical Optics Propagation was used to evaluate the magnitude of the spot irradiance at both the center and corner of the print field. Both spot irradiance profiles are shown normal to the image plane in the figure below.

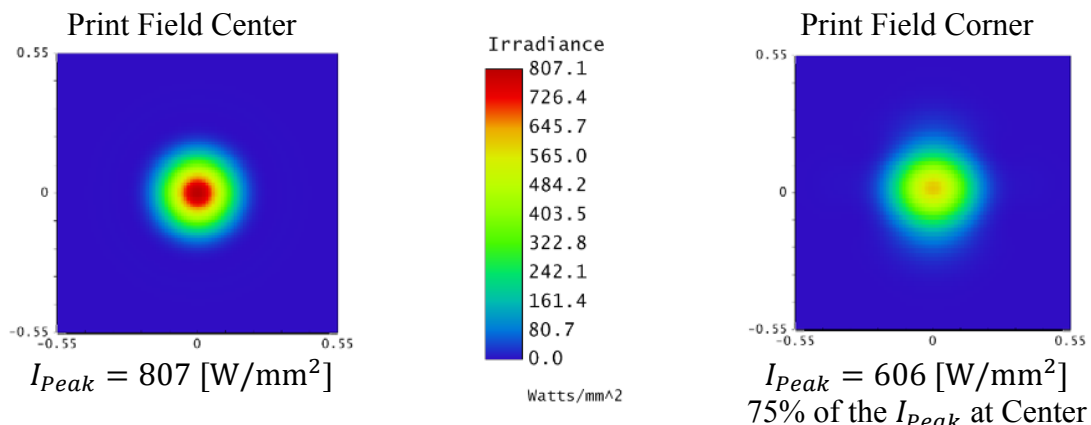


Figure 27: POP results for spots at the center (left) and corner (right) of the *Simplified System* image field.

Based on the peak irradiance equation, the anticipated peak irradiance for the spot at the center of the image should be $\sim 775 \text{ W/mm}^2$, and the corner peak irradiance $\sim 666 \text{ W/mm}^2$. The POP results above are reasonably. The difference in values can be attributed to the inclusion of the

entire beam irradiance in the POP analysis (not just the $1/e^2$ diameter) and the vignetting effect of the apertures on the beam irradiance (more noticeable as the beam approaches the lens mount).

2.4.2 Scanning System

The second system analyzed included scan mirrors. The model was non-symmetric and 3-Dimensional. The scan mirrors were included in the Lens Editor as mirror surfaces, approximated as ellipses, and oriented at angles defined by Coordinate Breaks¹⁸. The mirror tilt, and the resulting system field of view, was defined by 17 Configurations comprised of paired tilt angles in various combinations of 0°, +/- 5°, +/- 6°, and +/- 11 ° (mechanical)¹⁹. The stop was located half-way between the scan mirrors, but was not used functionally in the optimization or evaluation. The system was optimized over all 17 configurations using the optimization process previously described. The optimized layout is shown in the figure below.

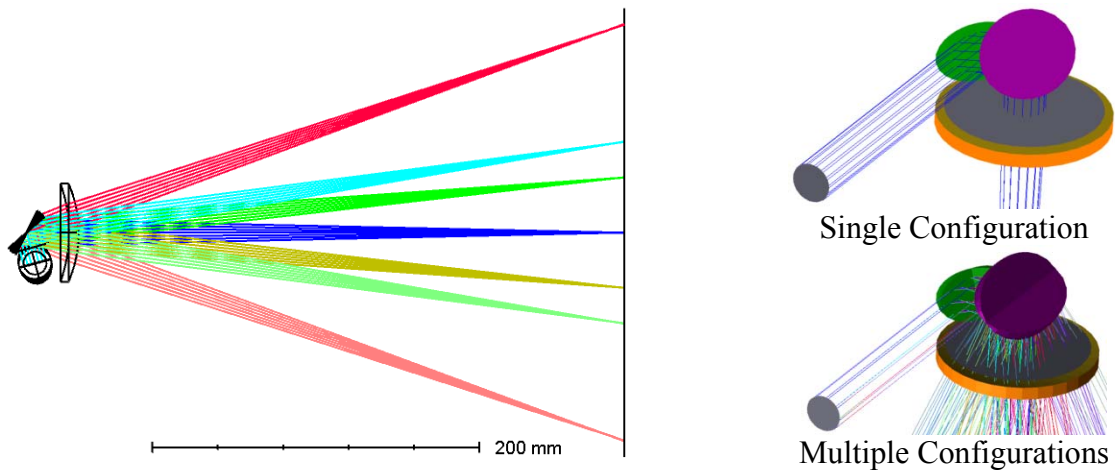


Figure 28: Layout for the *F-Theta Scanning System*. **Configurations** are represented by different colored ray bundles. The incident beam starts perpendicular to the page. Drawings to right show close up of X (green) and Y (pink) mirrors.

2.4.2.1 Results

The optimized system attributes are presented in the table below.

Table 10: Optimal geometry for the *Scanning System*

Scanning System Geometry								
Laser	Mirror - X	Stop	Mirror - Y	Lens Mount	First Surface	Second Surface	Image	
Thickness [mm]:	∞	9.625	9.625	20.477	5.35	5.862	333.797	
Radius [mm]:	∞	∞	∞	∞	-86.864	-75.769	∞	
Semi Diameter [mm] :	10x15	12	25x15	30	30	137	∞	
Focal Length [mm]:	n/a	n/a	n/a	n/a	n/a	323.411	n/a	
Lens Power [mm ⁻¹]:	n/a	n/a	n/a	n/a	n/a	0.00309	n/a	
Edge Thickness [mm]:	n/a	n/a	n/a	n/a	n/a	5.00	n/a	

The evaluation of third order aberrations using the Seidel and Structural coefficients presented in the previous section is predicated on an axial symmetric system. This system is no longer axially symmetric so only the performance metrics defined in the Constraints and Requirements section will be evaluated. The existence of aberrations was manifested indirectly in the irradiance profiles, spot diagrams, and distortion plots.

The diffraction encircled energy of a spot at both the center and edge of the print field are shown in the figure below.

¹⁸ the offset from the scanner axis to mirror face was not included

¹⁹ The optical deflection of the beam is 2x the mechanical deflection of the mirrors

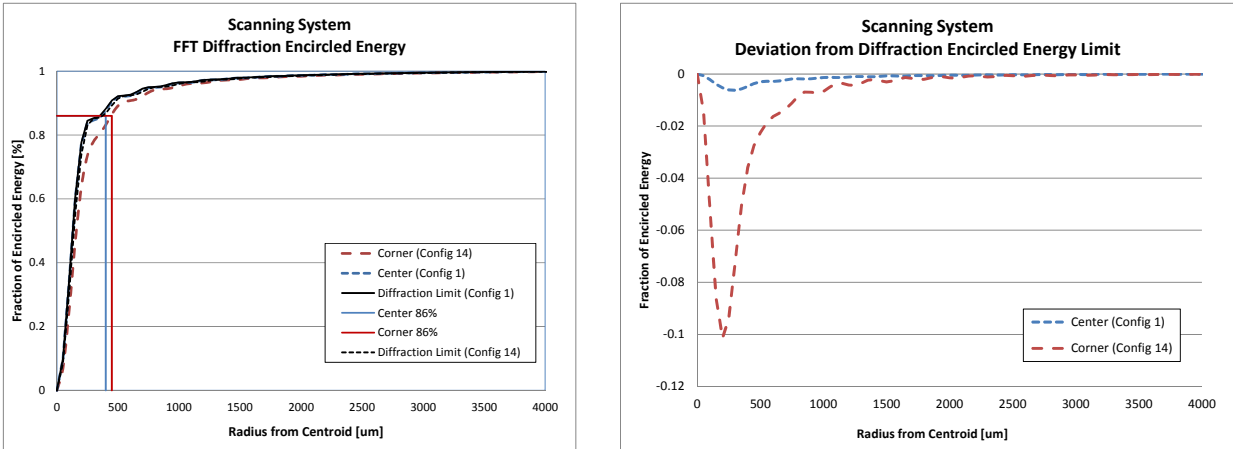


Figure 29: Diffraction encircled energy of the *Scanning System* compared to the diffraction limit. The system is within 1% at the print field center and 10% at the print field corner.

The plot to the right shows the difference between the predicted system performance and the diffraction limit. The encircled energy at both the center and corner of the print field is within 10% of the diffraction limit which does not meet the requirements.

The Huygens PSF cross sections, shown in the Figure below, indicate the peak irradiance for a spot in the corner of the print field should be ~17% of a spot located at the center of the image. This value indicates the irradiance uniformity over the print field is lower than predicted by the Symmetric system.

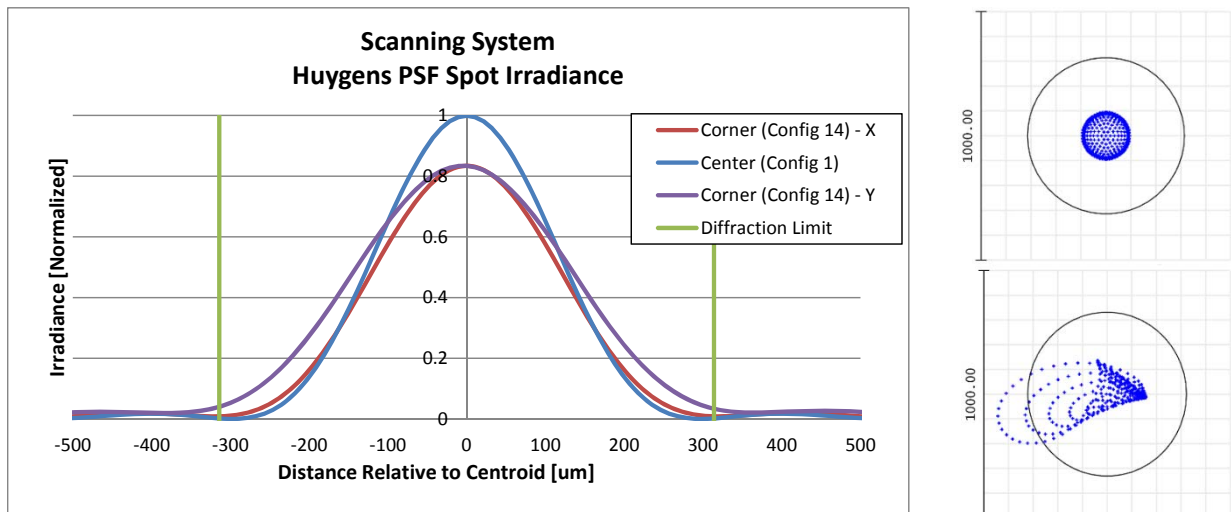


Figure 30: Huygens PSF Spot Irradiance of the *Scanning System* (left), spot diagrams displayed with the Airy disk of the rays at the print field center (top right), and corner (bottom right)

The spot diagrams are useful in illustrating the astigmatism and coma present in the corner of the print field. The spot diagrams are larger than those produced by the symmetric system; however they are still within the Airy disk, indicating the system is near the diffraction limit. To obtain an accurate spot size the effects of diffraction must be included.

Physical Optics Propagation was used to evaluate the magnitude of the spot irradiance at both the center and corner of the print field. Both spot irradiance profiles are shown normal to the image plane in the figure below.

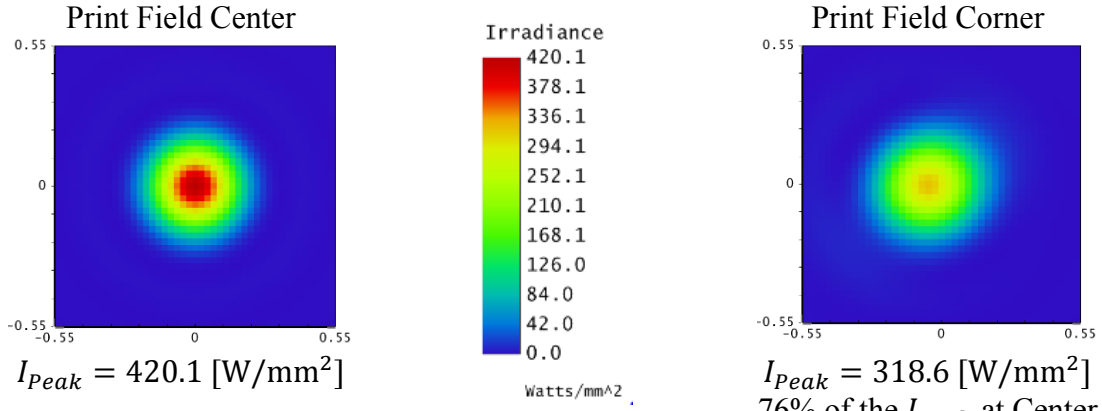


Figure 31: POP results for spots at the center (left) and corner (right) of the *Scanning System* print field.

The on axis peak irradiance is much lower than the value predicted by the peak irradiance equation and the *Simplified System* POP evaluation. The lower overall irradiance can be attributed to the mirror aperture size which is on par with the $1/e^2$ beam diameter (depending on orientation) and would therefore lose at least 13.5% of the beam power from the Gaussian tails. The Center to corner irradiance varies approximately 24% which is on par with what was predicted by the PSF cross sections.

2.4.2.2 Distortion Correction

A macro was created to evaluate distortion in the print field with and without the application of a correction file. A copy of the macros can be found in Appendix A3. The macro works in conjunction with a specific Zemax file. When the macro is executed, a text file with the mirror angles and spot locations for both the ideal, distorted, and corrected checkerboard spot pattern on the print field is created. The macro was required to be run once before the correction equations could be developed (development of the equations required knowledge of the system distortion).

The equations were developed by recording the separable X and Y components of transverse distortion at each sample location ($\Delta\bar{X}_{spot}$ and $\Delta\bar{Y}_{spot}$, respectively). The positional distortion was converted into angular distortion ($\Delta\theta_X$ and $\Delta\theta_Y$, respectively) based on a magnification factor that related the distance from the mirror to the rear principle plane location:

$$X_{Mag} = 1 + \frac{\bar{X}_{mirror}}{\bar{P}'}$$

$$Y_{Mag} = 1 + \frac{\bar{Y}_{mirror}}{\bar{P}'}$$

The X and Y angles along with X and Y angular distortion at each node were input to Matlab. Two polynomials were created using the curve fit (cftool) application to compensate for distortion in both the X and Y direction. The polynomials were created to maximize the accuracy

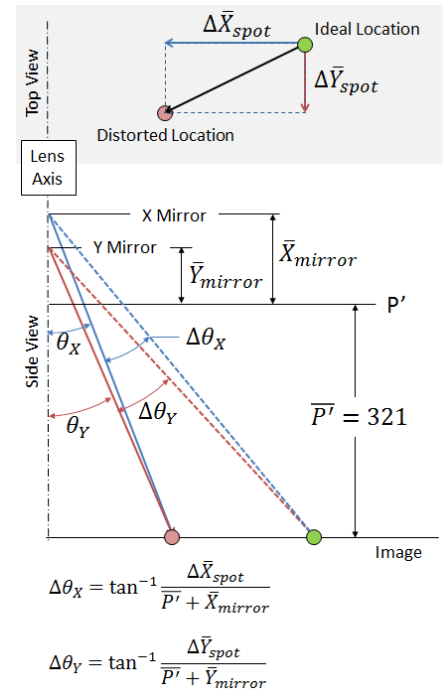


Figure 32: Diagram illustrating the conversion of position to angular distortion.

while minimizing the number of terms. The polynomial fit was created with the Linear Least Squares algorithm embedded in Matlab. The polynomials fit to the data perfectly (residual value of 1). Therefore, any error in the functionality of the polynomials would be related to the conversion of the transverse spot position error to angular error.

The approach above yielded acceptable results for distortion correction across the print field defined by the full deflection angle of the scanners²⁰ but was not optimized for the '+' shaped print field. An iterative process was used to adjust the magnification until distortion correction within the '+' shade field was optimized. The optimized magnification values and polynomial are presented in the table below.

Table 11: Correction equation polynomials and their coefficients for the Scanning System		
X Equation		
X Magnification = 1.109		
$f(x,y) = p00 + \mathbf{p10*x} + p01*y + p20*x^2 + p11*x*y + p02*y^2 + \mathbf{p30*x^3} + p21*x^2*y + \mathbf{p12*x*y^2}$		
X Coefficients		
p00 = 2.216E-17		p02 = 4.258E-19
p10 = 0.2612		p30 = 0.0003836
p01 = -1.228E-17		p21 = 5.794E-19
p20 = 2.134E-18		p12 = -0.0008603
p11 = -3.352E-18		
Y Equation		
Y Magnification = 1.054		
$f(x,y) = p00 + p10*x + \mathbf{p01*y} + p20*x^2 + p11*x*y + p02*y^2 + \mathbf{p21*x^2*y} + p12*x*y^2 + \mathbf{p03*y^3}$		
X Coefficients		
p00 = 2.618E-17		p02 = 4.539E-19
p10 = 4.494E-18		p21 = 0.0002808
p01 = 0.1593		p12 = -9.74E-20
p20 = -1.373E-18		p03 = 0.0003706
p11 = -1.508E-18		

The most influential terms in the polynomial are highlighted in bold. The terms correspond to the odd order terms of the variable being corrected. The 1st order corresponds to tilt, and the 3rd order corresponds to distortion. (23) The equations above were applied to the system and the results are shown in the figure below.

²⁰ This included correcting locations on the image plane that were outside the required print field and vignette by the lens mount.

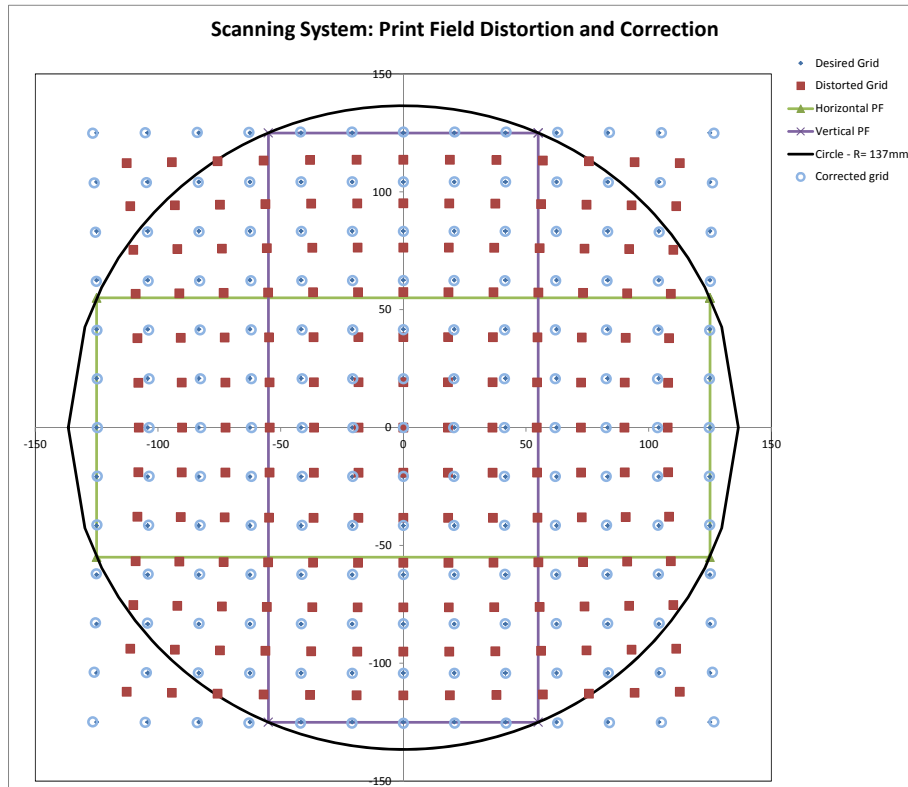


Figure 33: *Scanning System* ideal print field overlaid with distorted and corrected image. The magnification factor was adjusted to minimize the error in the + shaped print field. This came at the cost of increasing the error for the spots located outside the desired print field which would be vignetted by the lens mount aperture (black circle)

The corrected system is least accurate at the print field peripherals. The accuracy of the corrected system along the top and right side of the + shaped image is shown below.

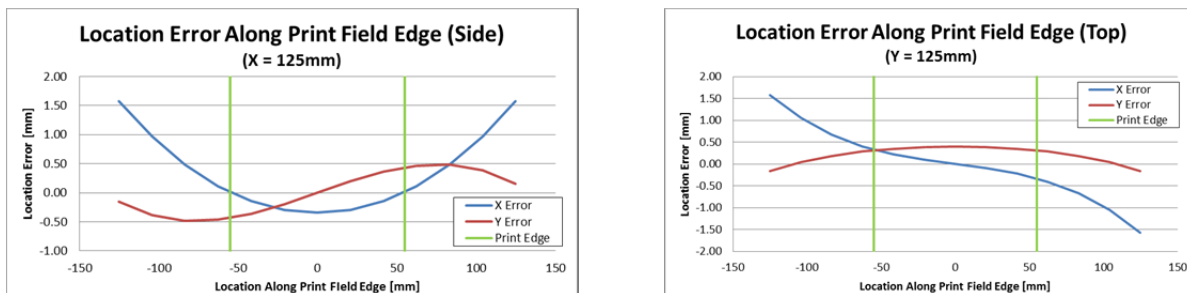


Figure 34: Accuracy of the corrected *Scanning System* along the print field edges.

The accuracy of the corrected grid was within ± 0.5 mm, which meets the specifications. The mirror deflection required to achieve the correction was checked, and found to be 10.76° and 10.94° (mechanical) for the X and Y mirrors, respectively. The mirror travel necessary for distortion correction was within the $\pm 11^\circ$ (mechanical) specifications.

2.4.3 Aspheric Scanning System

The *Aspheric Scanning System* added an aspheric surface to the lens optimized in the *Scanning System*. The Zemax functionality *Find Best Asphere* was used to determine the best surface to make aspheric, and then determine the values. The surface was optimized as an even 8th order asphere. The 2nd order term was not needed as this was defined by the surface radius. The 4th order term was used in lieu of the conic constant as their effects are extremely similar. Higher order terms were excluded in order to reduce cost and complexity. (24)

The system layout appears the same as the *Scanning System* layout. The *Aspheric Scanning* Zemax was optimized over all 17 configurations using the optimization process previously described. The results of the optimized system are presented in the next section.

2.4.3.1 Results

Zemax determined the second surface was the best surface to make aspheric. The optimized system attributes are presented in the table below.

Table 12: Optimal geometry for Aspheric Scanning System

Aspheric Scanning System							
Laser	Mirror - X	Stop	Mirror - Y	Lens Mount	First Surface	Second Surface	Image
Thickness [mm]:	∞	9.625	9.625	20.477	5.34	5.821	336.038
Radius [mm]:	∞	∞	∞	∞	-82.078	-72.471	∞
Semi Diameter [mm]:	10x15	12	25x15	30	30	137	∞
Focal Length [mm]:	n/a	n/a	n/a	n/a	n/a	326.057	n/a
Lens Power [mm ⁻¹]:	n/a	n/a	n/a	n/a	n/a	0.00307	n/a
Edge Thickness [mm]:	n/a	n/a	n/a	n/a	n/a	5.00	n/a
Conic	n/a	n/a	n/a	n/a	n/a	0.00	n/a
4th	n/a	n/a	n/a	n/a	n/a	4.47790E-08	n/a
6th	n/a	n/a	n/a	n/a	n/a	-8.46966E-11	n/a
8th	n/a	n/a	n/a	n/a	n/a	4.20237E-14	n/a

The X and Y Curvature of the aspheric surface is shown in the figure below. The curvature varies with pupil coordinate allowing additional degrees of freedom to correct aberrations.

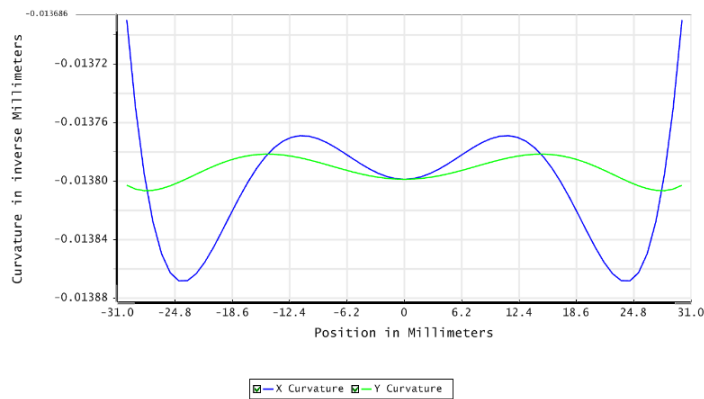


Figure 35: X and Y curvature of the aspheric as seen by the on-axis configuration.

The diffraction encircled energy of a spot at both the center and edge of the print field are shown in the figure below.

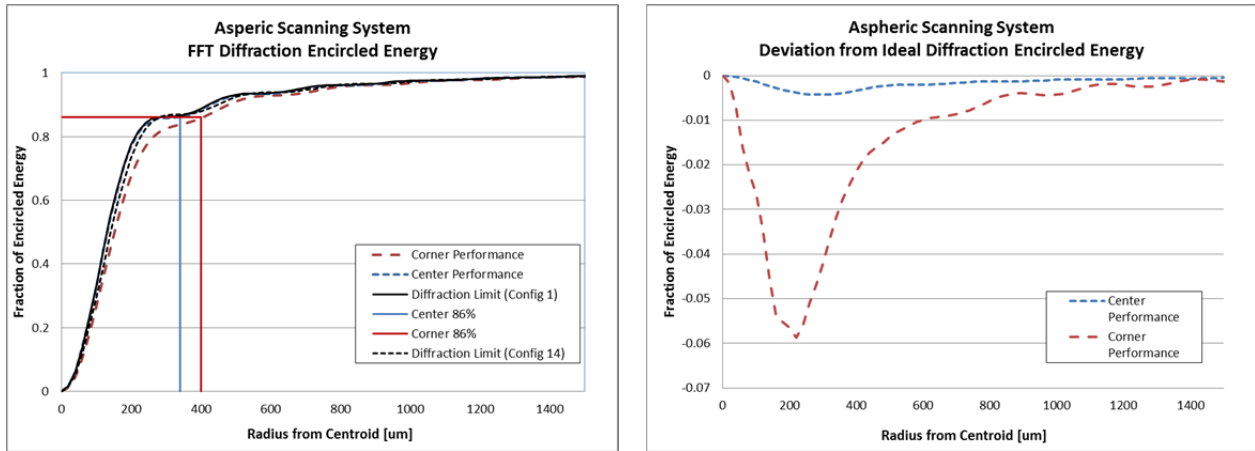


Figure 36: Diffraction encircled energy of the *Aspheric Scanning System* compared to the diffraction limit. The system is within 1.0% at the print field center and 6.0% at the print field corner.

The plot to the right shows the difference between the predicted system performance and the diffraction limit. The encircled energy at both the center and corner of the print field is within 6% of the diffraction indicating the aspheric surface did indeed increase the system performance compared to spherical surfaces alone.

The Huygens PSF cross sections, shown in the figure below, indicate the peak irradiance for a spot in the corner of the image should be $\sim 20\%$ of a spot located at the center of the image. This value indicates the irradiance uniformity over the image is lower than predicted by the *Simplified System* but $\sim 3\%$ higher than for the *Scanning System*.

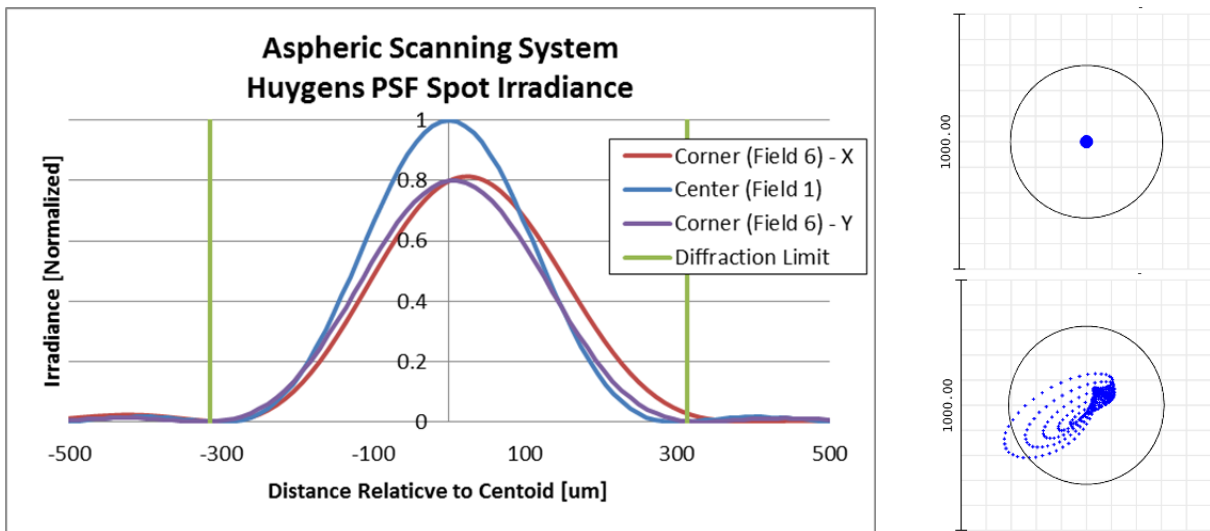


Figure 37: Huygens PSF cross sections of Spot Irradiance (left), spot diagrams displayed with the Airy disk of the rays at the print field center (top right), and corner (bottom right) for the *Aspheric Scanning System*

The spot diagrams are useful in illustrating the astigmatism and coma present in the corner of the print field. The spots are approximately the same size as in the *Scanning System*; and they are within the Airy disk, indicating the system is near the diffraction limit. To obtain an accurate spot size the effects of diffraction must be included.

Physical Optics Propagation was used to evaluate the magnitude of the spot irradiance at both the center and corner of the print field. Both spot irradiance profiles are shown normal to the image plane in the figure below.

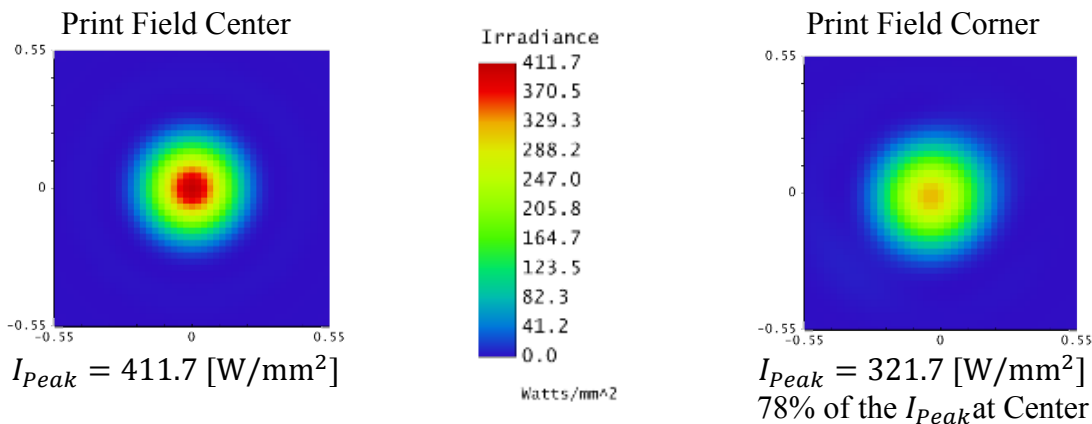


Figure 38: POP results for spots at the center (left) and corner (right) of the *Aspheric Scanning System* print field.

The center peak irradiance is slightly less than the *Scanning System* (due to a slightly longer focal length), but the corner irradiance is higher. The *Aspheric Scanning System* has numerically better irradiance uniformity; however the value is small (less than ~2%) and is likely to be indiscernible during the functional evaluation of the lens.

2.4.3.2 Distortion Correction

The same macro used to evaluate the *Scanning System* was used for this system. Minor changes to the code were made to account for the different physical geometry. The same process was followed, and the correction equation results are presented in the table below.

Table 13: Correction equation polynomials and their coefficients for the <i>Aspheric Scanning System</i>	
X Equation	
X Magnification = 1.109	
$f(x,y) = p00 + \mathbf{p10*x} + p01*y + p20*x^2 + p11*x*y + p02*y^2 + \mathbf{p30*x^3} + p21*x^2*y + \mathbf{p12*x*y^2}$	
X Equation Coefficients	
p00 = -3.337E-17	p02 = 4.731E-20
p10 = 0.2522	p30 = 0.000371
p01 = 1.705E-17	p21 = -4.771E-19
p20 = 3.807E-19	p12 = -0.0008539
p11 = 2.552E-19	
Y Equation	
Y Magnification = 1.054	
$f(x,y) = p00 + p10*x + \mathbf{p01*y} + p20*x^2 + p11*x*y + p02*y^2 + \mathbf{p21*x^2*y} + p12*x*y^2 + \mathbf{p03*y^3}$	
X Equation Coefficients	
p00 = -1.49E-17	p02 = 9.487E-20
p10 = -2.787E-19	p21 = 0.00027
p01 = 0.1534	p12 = 6.814E-20
p20 = 4.518E-19	p03 = 0.0003565
p11 = 3.277E-18	

The most influential terms in the polynomial are highlighted in bold. The terms correspond to the odd order terms of the variable being corrected. The 1st order corresponds to tilt, and the 3rd order

corresponds to distortion. (23) The equations above were applied to the system and the results are shown in the figure below.

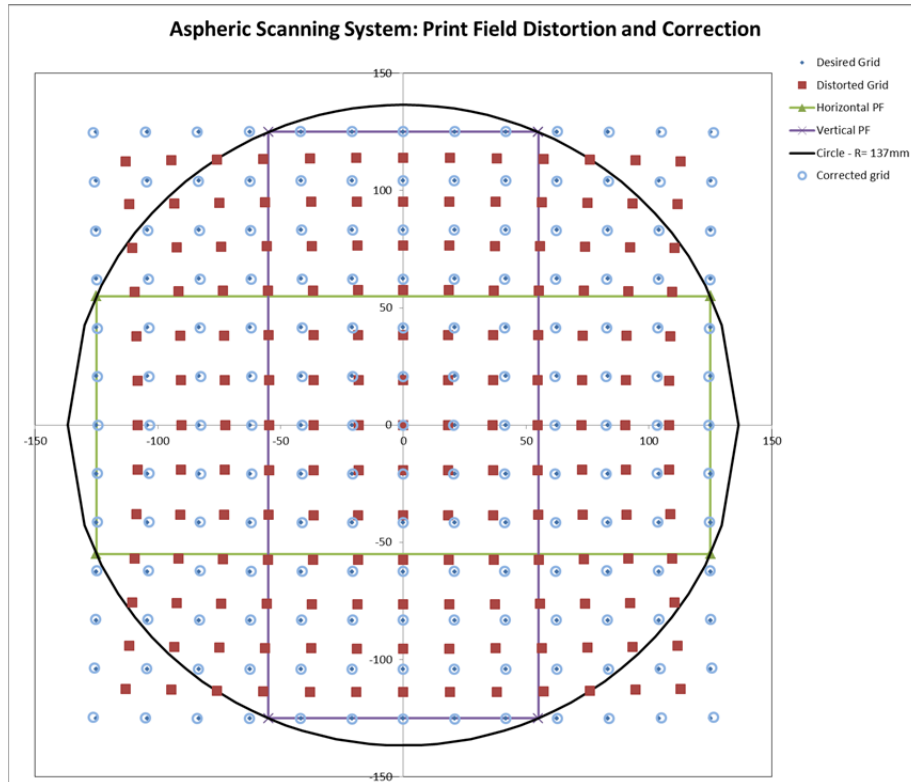


Figure 39: *Aspheric Scanning System* ideal print field overlaid with distorted and corrected image. The magnification factor was adjusted to minimize the error in the + shaped print field. This came at the cost of increasing the error for the spots located outside the desired print field which would be vignetted by the lens mount aperture (black circle)

The corrected system is least accurate at the image peripherals. The accuracy of the corrected system along the top and right side of the + shaped print field is shown below.

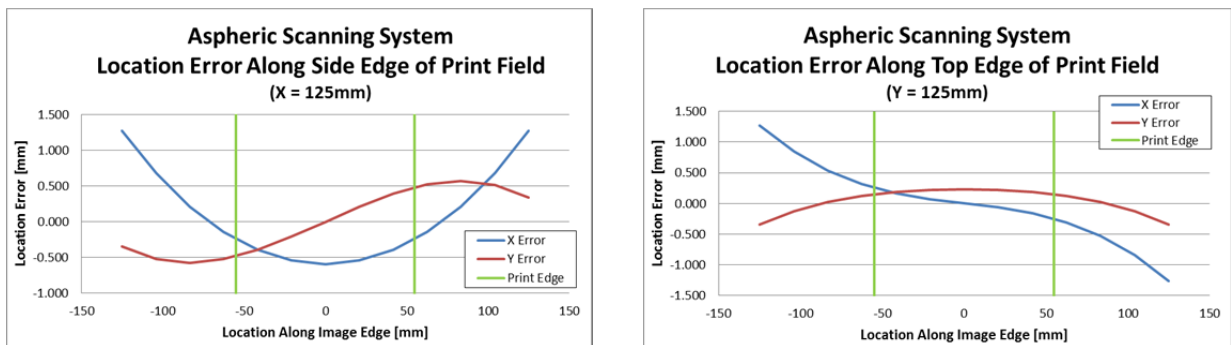


Figure 40: Accuracy of the corrected *Aspheric Scanning System* along the print field edges.

The accuracy of the corrected grid was within ± 0.6 mm, which meets the specifications. The mirror deflection required to achieve the correction was checked, and found to be 10.63° and 10.81° (mechanical) for the X and Y mirrors, respectively. The mirror travel necessary for distortion correction was within the $\pm 11^\circ$ (mechanical) specifications.

2.4.4 F-Theta Simplified System

This system was based on the *Simplified System*. The physical layout was the same; however the fields were defined by angles in objects space instead of image coordinates. The angles used were 0°, 5.0°, 10.0°, 15.0°, 20.0°, and 24.9° (optical). The image coordinate for each field angle was calculated based on the F-Theta criteria and the Merit function was edited to include operands to locate the centroid of the fields to the calculated f -Theta value.

The system was then optimized with a single element. The f -Theta criteria was met, but the spot size was unacceptably large. Repeated attempts to optimize a single lens to meet the spot size and f -Theta criteria failed. An additional lens was added to increase the degrees of freedom. The two element system was then optimized, and found capable of meeting all criteria including f -Theta. The *F-Theta Simplified System* is shown the figure below.

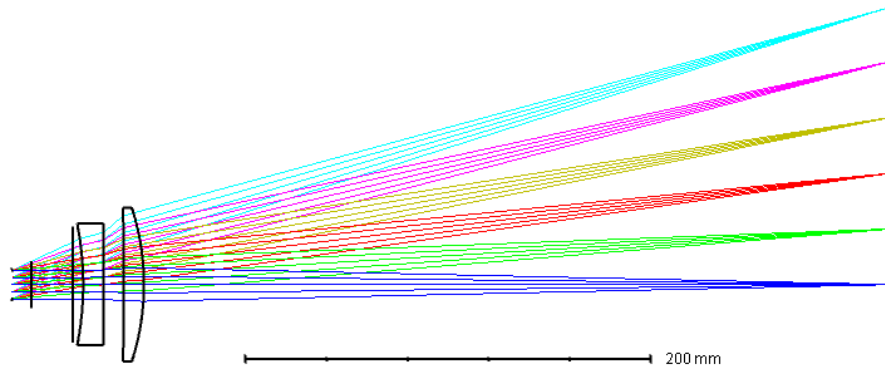


Figure 41: Layout for the *F-Theta Simplified System*. **Fields** are represented by different colored ray bundles.

2.4.4.1 Results

The optimized system attributes are presented in the table below.

Table 14: Optimal geometry for *F-Theta Simplified System*

F-Theta Simplified System								
Stop	Phantom	Lens Mount	First Surface	Seceond Surface	First Surface	Second Surface	Image	
Thickness [mm]:	9.625	20.477	5	10.001	10.014	10.002	369.455	
Radius [mm]:	∞	∞	-152.171	4123.405	-22202.4	-122.59	∞	
Semi Diameter [mm] :	10x15	12	30	30	38	38	138	
Focal Length [mm]:	n/a	n/a	n/a	-104.483	n/a	92.29	n/a	
Lens Power [mm ⁻¹]:	n/a	n/a	n/a	-0.00957	n/a	0.01084	n/a	
Edge Thickness [mm]:	n/a	n/a	n/a	13.10	n/a	4.29	n/a	
System Focal Length [mm]							314.9	
System Power [mm ⁻¹]							0.00318	

The total system aberrations in terms of waves are summarized in the table below.

Table 15: Sum of Aberrations in the *F-Theta Simplified System* at the image

Spherical	Coma	Astigmatism	Petzval Field Curvature	Distortion	Defocus	Tilt / Magnification
W040	W131	W222	W220P	W311	W020	W111
0.0229	-0.0864	-0.2551	0.1293	18.7918	0	0

The aberration contribution of each surface in the system is shown in the Figure below.

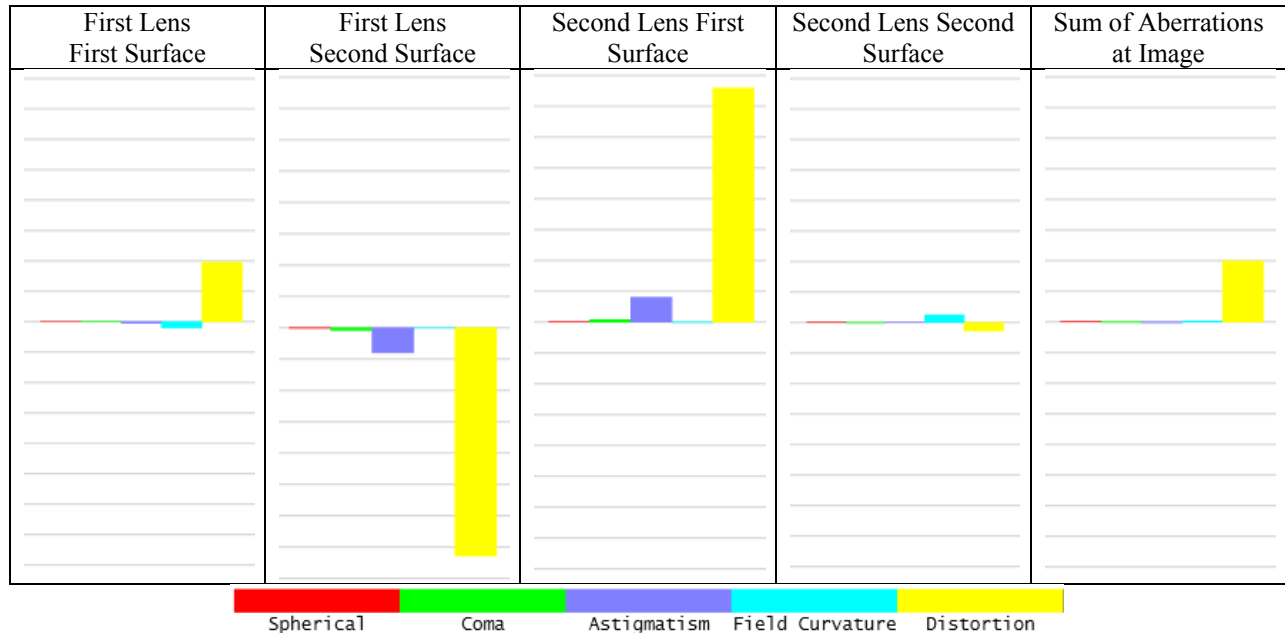


Figure 42: Aberrations at each surface of the *F-Theta Simplified System* Scale is 200um / horizontal bar. The max total distortion is ~1.6 mm, the net sum is ~0.4 mm at the image.

The astigmatism and distortion dominate system aberrations. Distortion was a necessary aberration to meet the *f*-Theta criteria. The astigmatism, mostly canceled out through the system, as did the other aberrations.

The image quality, as measured by the diffraction encircled energy, at both the center and edge of the field are shown in the figure below.

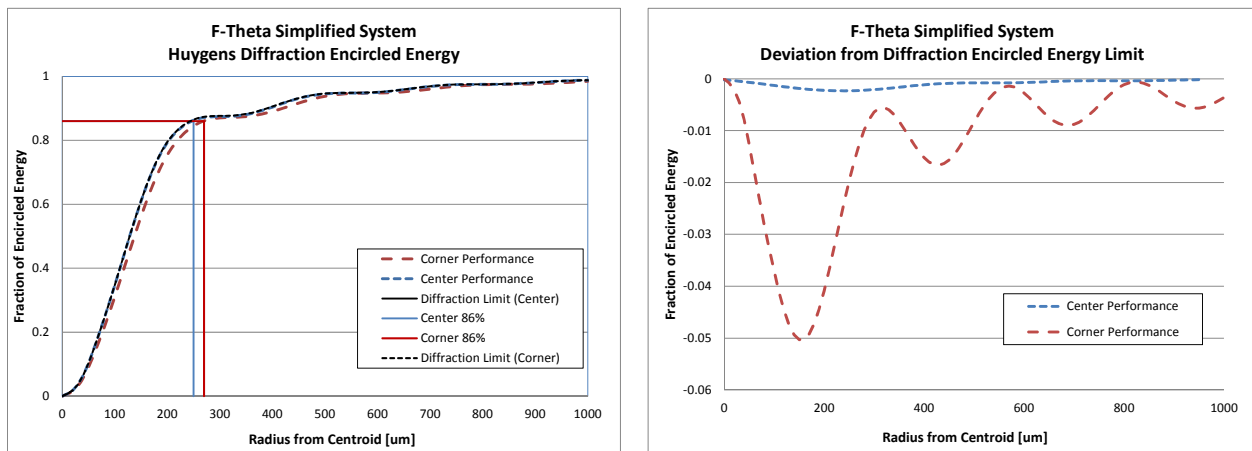


Figure 43: Diffraction encircled energy of the *F-Theta Simplified System* compared to the diffraction limit. The system is within 1% at the print field center and 5.0% at the print field corner

The plot to the right shows just the difference between the predicted system performance and the diffraction limit. The encircled energy at both the center and corner of the print field is within 5% of the diffraction limit, which meets the requirement.

The Huygens PSF cross sections, shown in the figure below, indicate the peak irradiance for a spot in the corner of the image should be ~9% of a spot located at the center of the print field. This value indicates the irradiance uniformity over the print field is better than all other systems evaluated to this point.

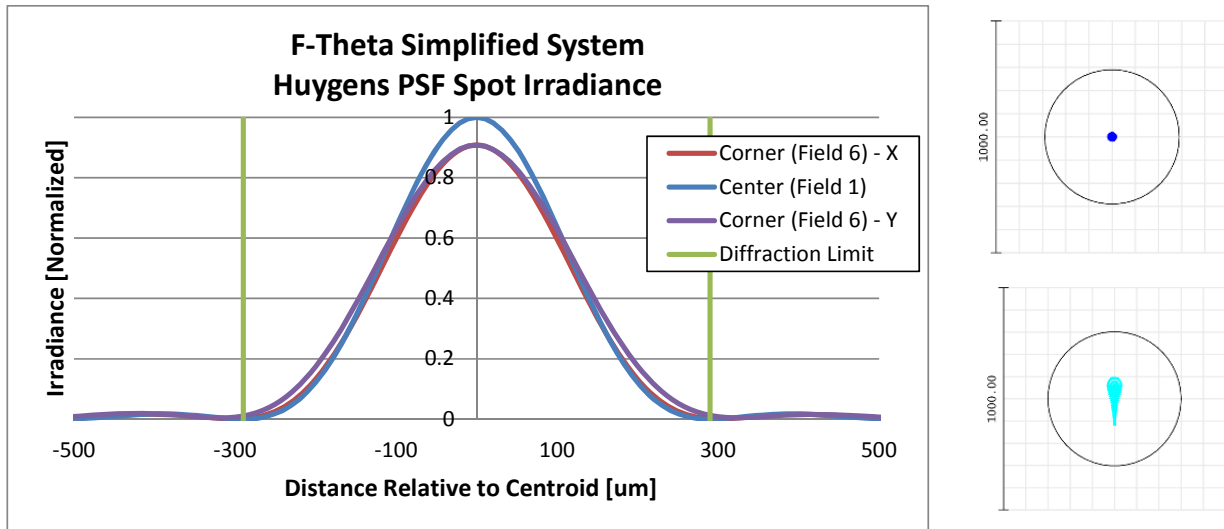


Figure 44: Huygens PSF Spot Irradiance (left), spot diagrams displayed with the Airy disk of the rays at the print field center (top right), and corner (bottom right)

The spot diagrams and the resulting radii of the ray bundles as they appear on the image plane are well within the Airy disk. The spot shapes are useful in illustrating the astigmatism in the corner of the print field.

Physical Optics Propagation was used to evaluate the magnitude of the spot irradiance at both the center and corner of the print field. Both spot irradiance profiles are shown normal to the image plane.

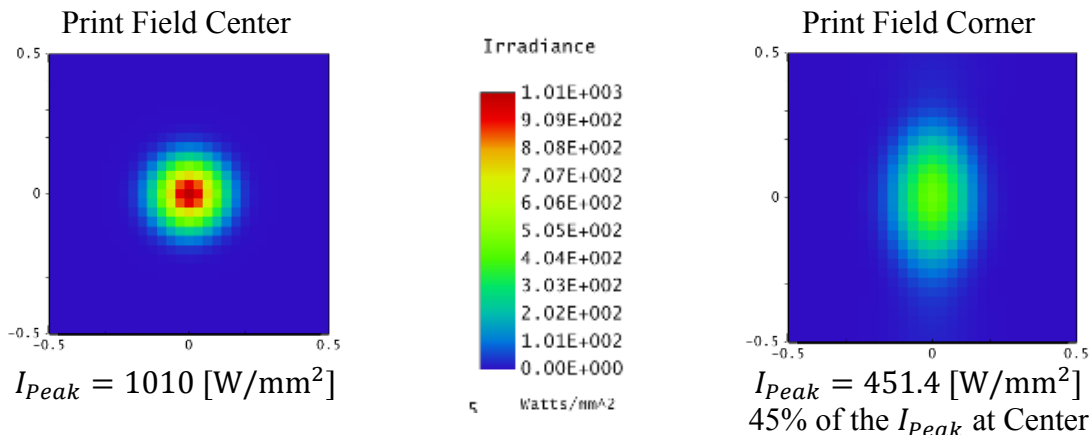


Figure 45: POP results for spots at the center (left) and corner (right) of the *F-Theta Simplified System* print field.

This irradiance at the print field center is much higher than expected. The magnitude of the irradiance at the print field corner is on par with the values predicted by previous systems.

The system performance with respect to meeting the *f*-Theta criteria is shown in the table below. The criteria was met to within 0.2 % which was within the requirements.

Table 16: Results of the <i>F-Theta Simplified System</i> with respect to the <i>F-Theta</i> criteria.				
Object Field Angle [° Opt]	Required [mm]	Imaged [mm]	Difference	
			[mm]	[%]
0	0.00	0.00	0.00	0
5	27.50	27.44	0.06	0.22%
10	55.00	54.93	0.07	0.12%
15	82.50	82.51	-0.01	-0.01%
20	110.00	110.13	-0.13	-0.12%
24.9	137.00	137.05	-0.05	-0.04%

2.4.5 F-Theta Scanning System

This system was a hybrid between the *F-Theta Simplified System* and the *Scanning System*. The model started as a copy of the *Scanning System* with the addition of a 2nd element. The geometry of the lenses was then copied from the *F-Theta Simplified System*. The object field of view was controlled by the scan mirrors which were defined in separate configurations.

The Merit function was edited to include the X and Y coordinate constraints for each configuration to evaluate the *f-Theta* criteria during optimization. During the optimization process it was found best to constrain only one of the print field coordinates. Constraining both the X and Y proved counterproductive to the optimization. Meeting the *f-Theta* criteria for one mirror yielded acceptable results for the other mirror as well.

The two element system was then optimized and found capable of meeting all criteria including that imposed by the *f-Theta* constraint. The *F-Theta Scanning System* is shown the figure below.

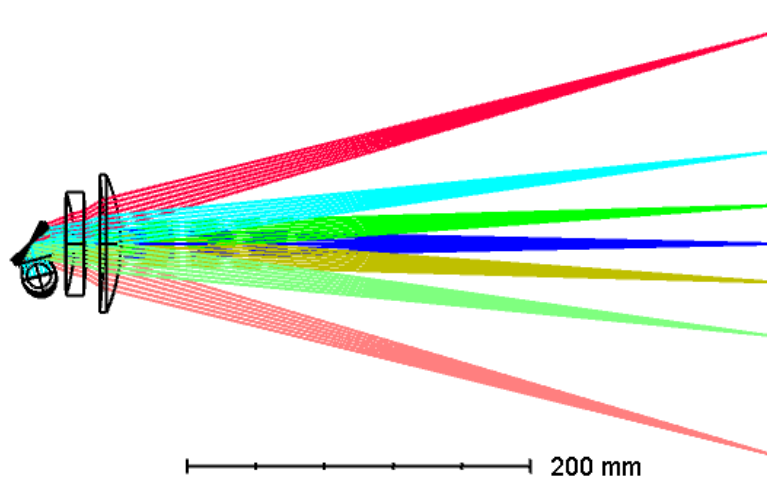


Figure 46: Layout for the *F-Theta Scanning System*. Configurations are represented by different colored ray bundles. The incident beam starts perpendicular to the page.

2.4.5.1 Results

The optimized system attributes are presented in the table below.

Table 17: Optimal geometry for the *F-Theta Scanning System*

F-Theta Scanning System										
Laser	Mirror - X	Stop	Mirror - Y	Lens Mount	First Surface	Second Surface	First Surface	Second Surface	Image	
Thickness [mm]:	∞	9.625	∞	20.477	5	7.022	10.039	10.006	382.413	
Radius [mm]:	∞	∞	∞	∞	∞	-97.245	-277.81	-360.799	-100.201	∞
Semi Diameter [mm]:	10x15	12	25x15	28.5	30	30	40	40	40	∞
Focal Length [mm]:	n/a	n/a	n/a	n/a	n/a	-109.145	n/a	96.7358	n/a	n/a
Lens Power [mm ⁻¹]:	n/a	n/a	n/a	n/a	n/a	-0.00916	n/a	0.01034	n/a	n/a
Edge Thickness [mm]:	n/a	n/a	n/a	n/a	n/a	10.14	n/a	4.53	n/a	n/a
System Focal Length [mm]:										322.997
System Power [mm ⁻¹]:										0.00310

The image quality, as measured by the diffraction encircled energy, at both the center and edge of the field are shown in the figure below.

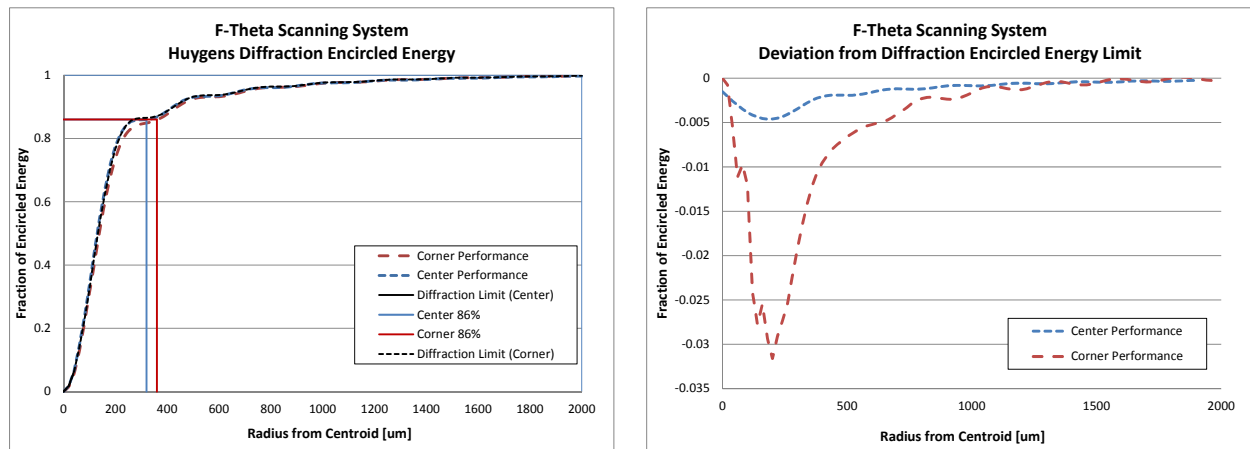


Figure 47: Diffraction encircled energy of the *F-Theta Scanning System* compared to the diffraction limit. The system is within 0.5% at the image print field center and 3.5% at the corner

The plot to the right shows just the difference between the predicted system performance and the diffraction limit. The encircled energy at both the center and corner of the print field is within 3.5% of the diffraction limit, and within the design requirements.

The cross section of the Huygens PSF, shown in the Figure below, includes the predicted diffraction limited spot size (297um). Both cross sections show irradiance normal to the image surface.

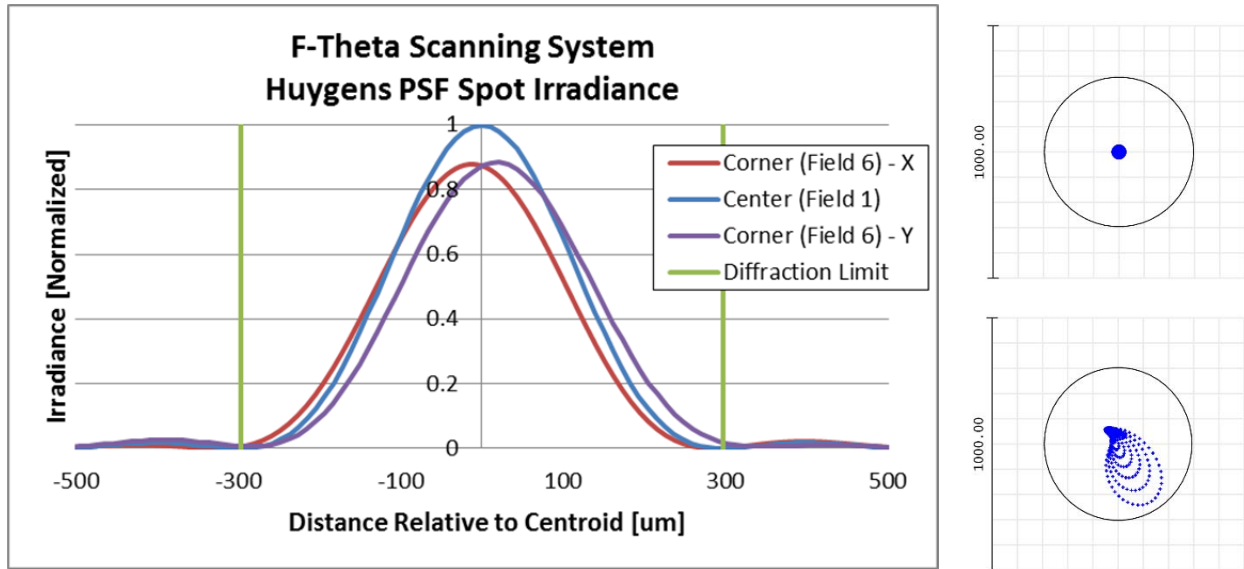


Figure 48: Huygens PSF Spot Irradiance (left), spot diagrams displayed with the Airy disk of the rays at the print field center (top right), and corner (bottom right) for the *F-Theta Scanning System*.

The spot diagrams and the resulting radii of the ray bundles as they appear on the image plane are well within the Airy disk. The spot shapes are useful in illustrating the astigmatism and coma in the corner of the print field. To obtain an accurate spot size the effects of diffraction must be included.

Physical Optics Propagation was used to evaluate the magnitude of the spot irradiance at both the center and corner of the print field. Both spot irradiance profiles are shown normal to the image plane.

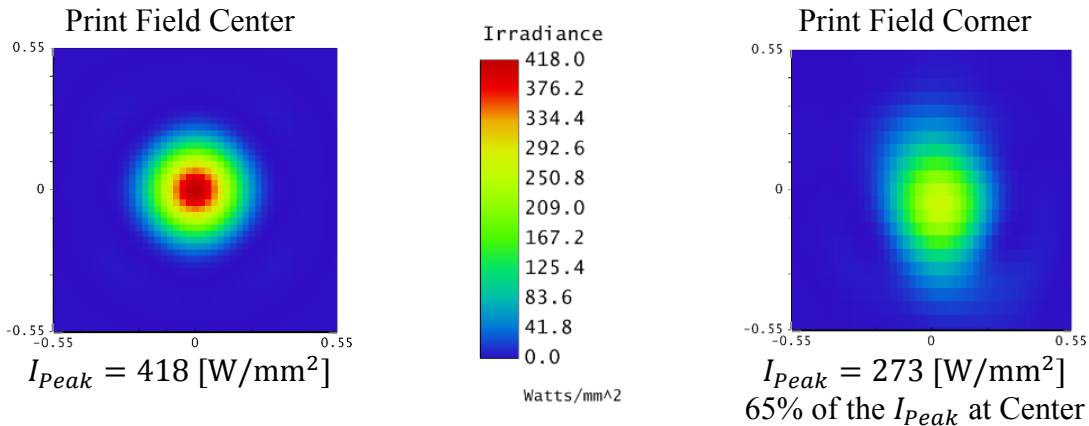


Figure 49: POP results for spots at the center (left) and corner (right) of the *F-Theta Scanning System* print field.

The irradiance of the print field corner is significantly lower than the print field center. This can be attributed to the lens mount apertures which vignette some incident light at the corners of the image at each lens in the system.

The print field met the *f*-Theta criteria within 5.0% as shown in the table below. The magnitude of the error is up to 2.5 mm, which does not meet the requirements.

Table 18: Results of the *F-Theta Scanning System* with respect to the *f-Theta* criteria.

Config	Object Field Angle		Y Scanner Data				X Scanner Data				
	Y	X	Required	Imaged	Difference		Required	Imaged	Difference		
	[° Me]	[° Me]	[mm]	[mm]	[mm]	[Abs %]	[mm]	[mm]	[mm]	[Abs %]	
1	0	0	0.00	0.00	0.00	0	0.00	0.00	0.00	0	
2	2	2	22.55	22.42	0.13	0.59%	22.55	22.47	0.08	0.37%	
3	2	-2	22.55	22.42	0.13	0.59%	-22.55	-22.47	-0.08	0.37%	
4	-2	2	-22.55	-22.42	-0.13	0.59%	22.55	22.47	0.08	0.37%	
5	-2	-2	-22.55	-22.42	-0.13	0.59%	-22.55	-22.47	-0.08	0.37%	
6	5	11	56.37	53.88	2.49	4.42%	124.02	125.15	-1.13	0.91%	
7	5	-11	56.37	53.88	2.49	4.42%	-124.02	-125.15	1.13	0.91%	
8	-5	11	-56.37	-53.88	-2.49	4.42%	124.02	125.15	-1.13	0.91%	
9	-5	-11	-56.37	-53.88	-2.49	4.42%	-124.02	-125.15	1.13	0.91%	
10	11	5	124.02	123.48	0.54	0.44%	56.347	58.09	-1.74	3.09%	
11	11	-5	124.02	123.48	0.54	0.44%	-56.347	-58.09	1.74	3.09%	
12	-11	-5	-124.02	-123.48	-0.54	0.44%	-56.347	-58.09	1.74	3.09%	
13	-11	5	-124.02	-123.48	-0.54	0.44%	56.347	58.09	-1.74	3.09%	
14	4	4	45.093	44.7	0.39	0.87%	45.09	45.13	-0.04	0.08%	
15	4	-4	45.093	44.7	0.39	0.87%	-45.09	-45.13	0.04	0.08%	
16	-4	4	-45.093	-44.7	-0.39	0.87%	45.09	45.13	-0.04	0.08%	
17	-4	-4	-45.093	-44.7	-0.39	0.87%	-45.09	-45.13	0.04	0.08%	
				Max =	2.49	4.42%			Max =	1.74	3.09%

3. Conclusion

This Thesis designed and evaluated 5 different scanning systems with respect to meeting requirements imposed by the marking system. The table below summarizes the results; parameters that failed to meet the requirements are shown in bold red text.

System	Metrics	<i>Simplified System</i>	<i>Scanning System</i>	<i>Aspheric Scanning System</i>	<i>F-Theta Simplified System</i>	<i>F-Theta Scanning System</i>	
Focal Length [mm]	Short	323.8	323.4	326.1	314.9	323.0	
Center Thickness [mm]	5 to 10	5.867	5.862	5.821	1 st - 10.0 2 nd - 10.00	1 st - 7.02 2 nd - 10.00	
Edge Thickness [mm]	<5 *10	5.09	5.00	5.00	1 st - 10.00 2 nd - 4.29	1 st - 10.14 2 nd - 4.53	
Lens Diameter [mm]	60 *Min	60	60	60	1 st - 60 2 nd - 76	1 st - 60 2 nd - 76	
Field Size ²¹	137	Met	Met	Met	Met	Met	
Irradiance [W/mm ²]	Center	Max	807	420	412	1010	428
	Corner	Max	606	319	322	451	276
	Difference	Min	75%	76 %	78 %	45 %	64 %
Deviation from Diffraction Limit	Center	<5%	< 1.0 %	< 1.0 %	< 1.0 %	< 1.0 %	< 0.05 %
	Corner		< 12.5 %	< 10 %	< 6.0%	< 5.0 %	< 3.5 %
	Average		< 6.75%	< 5.5%	< 3.5%	< 3%	< 2%
Position Accuracy [mm]	<1.1	n/a	+/- 0.5	+/- 0.6	+/- 0.1	+/- 2.5	
Cost	Min	n/a	\$	1.6 x \$	n/a	3x \$	

* denotes 2 Element system requirement

The exclusion of the two mirrors in the *Simplified System* and *F-Theta Simplified System* resulted in a drastic overestimation in the irradiance that would appear on the image plane. Modeling the system with the inclusion of the mirrors takes more time, but delivers more accurate results, particularly with respect irradiance though the system. However, modeling the system without the scan mirrors did prove far easier and faster and resulted in lens geometry very similar to the geometry of the more accurately modeled system. Creating a simplified system is a good starting point for future system analysis.

The *Scanning System* model contains the best performance to cost ratio. The single element meniscus scan lens required the development of correction equations to account for the distortion introduced by the system. The thesis described the process by which correction equations were developed and validated their accuracy. The deviation from the diffraction limit at the corner of the print field is a concern, however, on average; the system is operating within 5% of the diffraction limit over the entire print field.

The *Aspheric Scanning System* provides modest improvements over the *Scanning System* but is accompanied by higher cost. Manufacturing aspheric surfaces is becoming more common practice, and the cost difference between spherical and aspheric surface is likely to decrease in time.

²¹ Half diagonal = 137mm

The *F-Theta Scanning System* provided nearly diffraction limited performance across the print field; however that did not translate to irradiance uniformity. The large deviation in irradiance over the field indicated by the POP analysis would certainly be noticeable, and coupled with the higher cost, makes the system less appealing for the marking application.

For all the systems the effect of aberrations on irradiance was minimal due to the near diffraction limited performance. Additionally, the diffraction limit prevented any single system from drastically out performing any other system.

Appendix

A1: Useful Equations

Wavelength and Frequency Relation

$$\lambda = \frac{c}{\nu}$$

Where:

c	[m/s]	Speed of light (a constant $c=3.0 \times 10^8$ m/s in free space/vacuum)
ν	[1/s]	Frequency at which the photon is oscillating
λ	[m]	Wavelength is the distance (typically nm to μm scale) covered during a period of oscillation

Diffraction Limited Spot Size

The equation below can be used to estimate the spot size of a focused, Gaussian beam (11)

$$D_{spot} = \frac{4M^2\lambda f}{\pi D_{beam}}$$

Where:

D_{spot}	[μm]	The diameter of the focused spot at the center for the print field
M^2		The quality of the incident beam (typical values: 1.0 to 1.2 for this application)
λ	[μm]	The wavelength of the incident beam
f	[mm]	The focal length
D_{beam}	[mm]	The diameter of the incident beam

Lens Power and Focal Length (Lens Makers Formula for a Thick Lens in Air)

$$\phi = \frac{1}{f} = (n - 1) \left[\frac{1}{R_1} - \frac{1}{R_2} + \frac{(n - 1)d}{nR_1R_2} \right]$$

Where:

ϕ	[mm^{-1}]	The lens power
f	[mm]	Focal Distance
n		Index of refraction (wavelength dependent)
R_1	[mm]	Radius of curvature of the first surface
R_2	[mm]	Radius of curvature of the second surface
d	[mm]	Thickness of the lens along the axis (Center Thickness)

Surface Power

$$\phi_S = \frac{(n - 1)}{R_S}$$

Where:

ϕ_S	[mm^{-1}]	The surface power
n		Index of refraction (wavelength dependent)
R_S	[mm]	Radius of curvature of the surface (must use correct sign convention)

Surface Sag

$$h = R - \sqrt{R^2 - \frac{diameter^2}{4}} = R \left(1 - \cos \frac{\theta}{2}\right) \quad \text{and}$$
$$\frac{\theta}{2} = \text{asin} \left(\frac{d/2}{R} \right)$$

Where:

h	[mm]	The sag height
R	[mm]	Radius of curvature of the first surface
d	[mm]	Diameter of the Lens

Back Focal Distance

$$BFD = f - \frac{\phi_1 CT}{\phi n}$$

Where:

BFD	[mm]	The Back Focal Distance
f	[mm]	The lens focal length
ϕ_1	[mm ⁻¹]	The power of the first surface
ϕ	[mm ⁻¹]	The power of the lens
CT	[mm]	The center thickness of the lens
n		The index of refraction

RMS Spot Size (15)

$$RMS_R = \sqrt{\frac{1}{N} \sum_{i=1}^N [(\varepsilon_{Yi} - \bar{\varepsilon}_Y)^2 + (\varepsilon_{Xi} - \bar{\varepsilon}_X)^2]} \quad BFD = f - \frac{\phi_1 CT}{\phi n}$$

Where:

RMS_R	[mm]	Root Mean Square Radius of the spot
ε_{Yi}	[mm]	Y print field coordinate of the i ray
$\bar{\varepsilon}_Y$	[mm]	Centroid Y print field coordinate
ε_{Xi}	[mm]	X print field coordinate of the i ray
$\bar{\varepsilon}_X$	[mm]	Centroid X print field coordinate
i		Designates a single ray traced through the system
N		The total number of rays traced through the system

Lens Shape Factor

$$X = \frac{R_1 + R_2}{R_1 - R_2}$$

Where:

X		Shape factor (sometime referred to Codington shape factor)
R_1	[mm]	Radius of curvature of the first surface
R_2	[mm]	Radius of curvature of the second surface

A2: Seidel Coefficients

Table 20: Seidel Coefficients (7)			
Aberration	Wavefront Expansion	Spherical Contribution	Asphere Contribution
Spherical	$W_{040} = \frac{1}{8}(S_I + \delta S_I)$	$S_I = \left(-\sum A^2 y \Delta \left(\frac{u}{n}\right)\right)$	$\delta S_I = a$
Coma	$W_{131} = \frac{1}{2}(S_{II} + \delta S_{II})$	$S_{II} = \left(-\sum A \bar{A} y \Delta \left(\frac{u}{n}\right)\right)$	$\delta S_{II} = \frac{\bar{y}}{y} a$
Astigmatism	$W_{222} = \frac{1}{2}(S_{III} + \delta S_{III})$	$S_{III} = \left(-\sum \bar{A}^2 y \Delta \left(\frac{u}{n}\right)\right)$	$\delta S_{III} = \left(\frac{\bar{y}}{y}\right)^2 a$
Field Curvature	$W_{220} = \frac{1}{4}(S_{IV} + \delta S_{IV})$	$S_{IV} = (-\sum \mathcal{K}^2 P)$	$\delta S_{IV} = 0$
Distortion	$W_{311} = \frac{1}{2}(S_V + \delta S_V)$	$S_V = \left(-\sum \frac{\bar{A}}{A} [\mathcal{K}^2 P + \bar{A}^2 y \Delta \left(\frac{u}{n}\right)]\right)$	$\delta S_V = \left(\frac{\bar{y}}{y}\right)^3 a$
Where:			
A	Fractional area of incoming ray, derived from marginal ray attributes: $A = nu + nyc$		
y	Marginal ray height at surface		
$\Delta \left(\frac{u}{n}\right)$	Change in slope of the marginal ray at surface index: $\Delta \left(\frac{u}{n}\right) = \frac{u'}{n'} - \frac{u}{n}$		
u	Marginal ray slope at surface		
n	Index of refraction of the incident medium		
n'	Index of refraction of the subsequent refracting medium		
c	Curvature: $c = 1/R$		
\bar{A}	Fractional invariant of Chief Ray, derived from chief ray attributes: $\bar{A} = n\bar{u} + n\bar{y}c$		
\bar{y}	Chief ray height at surface		
\bar{u}	Chief ray slope at surface		
\mathcal{K}	Lagrange Invariant: $\mathcal{K} = n\bar{u}y - nu\bar{y}$		
P	Petzval sum term: $P = c\Delta(1/n) = c\left(\frac{1}{n'} - \frac{1}{n}\right)$		
ε or K	Ellipticity of an a spherical surface: $\varepsilon^2 = K$		
a	Aspheric contributions to Seidel sum: $a = -\varepsilon^2 c^3 y^4 \Delta n$ or: $a = -Kc^3 y^4 \Delta n$		

The ray trace data: \bar{y} , \bar{u} , y , and u are derived from the YNU ray trace thru the system. The marginal ray was parallel to the chief ray thru the stop and offset in height by the aperture radius. The rays (both chief and marginal) were progressed through the system using the following equations: (15)

Ray Height:	$y' = y + u't'$
Ray Angle:	$u' = \frac{nu + y\phi}{n'}$
Where:	
y'	Ray height at next surface
y	Ray height at current surface
u'	Ray slope from the current surface to the next surface [radians]
u	Ray slope incident to current surface [radians]
t'	Thickness between the current and next surface
n	Index of refraction of the incident medium
n'	Index of refraction between the current and next surface
ϕ	Power of the surface: $\phi = \frac{n'-n}{R}$ where R is the radius of the surface

A3: Optic Studio Macro for Print Field Distortion

```
!System has two scan mirror, focusing lens, and image plane (set at focal distance)
! 1. Input an angle for first mirror (Angle 1) : X
! 2. Input angle to second mirror (Angle 2) : Y
! 3. Update Zemax file
! 4. Read the X and Y value for the location of the chief ray on the image plane (Spot Diagram)
! 5. Save Angle 1 and Angle 2 (for mirrors) along with X and Y position coordinate to a text file
! 6. Repeat with new mirror angles
!     a.Can be calculated with a for loop
!     b.Can be input from text file.
```

```
! This section defines the X and Y mirror angle
```

```
! Inputs
```

```
! Lens Parameters for Scan Lens
```

```
! Lens parameters
```

```
    Lens_RF = -86.864
    Lens_RS = -75.77
    Lens_ct = 5.848
    Lens_Diam = 60
    Lens_FD = 323
    Lens_BFD = 333.797           #DISTANCE FROM LENS TO IMAGE
    RF_Sag = 5.34
```

```
!Size of The Field
```

```
    hpf_length = 125           #Y mirror FOV
    hpf_height = 125           #X mirror FOV
    hpf_diameter = SQRT(POWR(hpf_length,2)+POWR(hpf_height,2))
    pf_Y_size = 2*hpf_length
    pf_X_size = 2*hpf_height
```

```
! Number of squares / grid dimensions
```

```
    gs_X = 11
    gs_Y = 11
```

```
!Correction Files
```

```
!X coefficients
```

```
    aa = 2.216E-17
    ab = 0.2612
    ac = -1.228E-17
    ad = 2.134E-18
    ae = -3.352E-18
    af = 4.258E-19
    ag = 0.0003836
    ah = 5.794E-19
    aj = -0.0008603
```

```
!Y coefficients
```

```
    ba = 2.618E-17
    bb = 4.494E-18
    bc = 0.1593
    bd = -1.373E-18
    be = -1.508E-18
    bf = 4.539E-19
    bg = 0.0002808
    bh = -9.74E-20
    bj = 0.0003706
```

```
!
```

```

!General Calculations
! Calculating the lens "magnification"
XY_Space = 19.24
YLens_Mnt = 20.477
YLens_Space = YLens_Mnt + RF_Sag
Ave_Mag_distance = (YLens_Space+XY_Space)/2
Ave_Dist = Lens_FD + Ave_Mag_distance
X_Dist = Lens_FD + XY_Space + YLens_Space
Y_Dist = Lens_FD + YLens_Space
! Inserting Lens data into the Lens Data menu
#SETSURFACEPROPERTY [the surface to be altered], PARM, [new value], [row/field for value]
Lens_CF = 1/Lens_RF
Lens_CS = 1/Lens_RS
Lens_SDiam = Lens_Diam/2
!First Surface of Lens
    SETSURFACEPROPERTY 14, CURV, Lens_CF
    SETSURFACEPROPERTY 14, THIC, Lens_ct
    SETSURFACEPROPERTY 14, SDIA, Lens_SDiam
! Second Surface of Lens
    SETSURFACEPROPERTY 15, CURV, Lens_CS
    SETSURFACEPROPERTY 15, THIC, Lens_BFD
! the print field Diameter
    SETSURFACEPROPERTY 16, SDIA, 137
! Sets the distance from the Y mirror to the lens surface
    SETSURFACEPROPERTY 12, THIC, YLens_Mnt
    SETSURFACEPROPERTY 13, THIC, RF_Sag

Update          #this updates the zemax file with the new lens data

! Print grid Square size
X_delta = pf_X_size / (gs_X + 1)
Y_delta = pf_Y_size / (gs_Y + 1)
! Half the printfield coordinates
hpf_X = pf_X_size / 2
hpf_Y = pf_Y_size / 2

!This creates heading on text file
OUTPUT "locationThor_C.txt", APPEND
PRINT "X_Linear_A, Y_Linear_A, X_Corrected_A, Y_Corrected_A, X_Delta_A, Y_Delta_A, X_Linear_P, Y_Linear_P,
Y_Distorted_P, X_Distorted_P, Y_Corrected_P, X_Corrected_P"

!
!-----
!This section determines the location of the beam given the ideal location inputs

!This loop controls x value
For i, 0, gs_X+1, 1
!This loop control y value
For j, 0, gs_Y+1, 1
!This section fills out the X-Y Grid spot locations
    x_spot = -hpf_X + i * X_delta
    y_spot = -hpf_Y + j * Y_delta
!
!-----
!This section determines the uncorrected beam angle and the resulting spot in the printfield
!This section fills determines the X & Y angle for the spot above (atan returns value in radians)
x_angle = (180/3.141593)*atan(x_spot/X_dist)/2      #division of 2 because Optical angle is 2x mecahnical
y_angle = (180/3.141593)*atan(y_spot/Y_dist)/2
!This section determines the sign of the X & Y angle (POWR function returns asolute value)
    s_x = x_angle/ABS0(x_angle)

```

```

s_y = y_angle/ABS(y_angle)
! This section inputs the X and Y angle into the ZeMax Model
!SETSURFACEPROPERTY the surface to be altered (x=3, y=9), PARM, new angle, tilt about x = 3
  SETSURFACEPROPERTY 3, PARM, x_angle, 3
  SETSURFACEPROPERTY 9, PARM, y_angle, 3
UPDATE                                #this updates the Zemax file with the new angles
! This section finds the X and Y corrdinate of the beam
! E = OPEV(CX, surface, wave, field, polarization, sample #, 0)
  CXtemp = OCOD("CENX")
  Xposition = OPEV(CXtemp, 16, 0, 1, 0, 10, 0)
  CYtemp = OCOD("CENY")
  Yposition = OPEV(CYtemp, 16, 0, 1, 0, 10, 0)

!
!-----!
!This section determines the corrected beam angle and the resulting spot in the print field
!This section determines the corrected X & Y angle for the spot above
  x_NADelta = aa + ab*x_angle + ac*y_angle + ad*POWR(x_angle,2) + ae*x_angle*y_angle +
af*POWR(y_angle,2) + ag*s_x*POWR(x_angle,3) + ah*POWR(x_angle,2)*y_angle + aj*x_angle*POWR(y_angle,2)
  y_NADelta = ba + bb*x_angle + bc*y_angle + bd*POWR(x_angle,2) + be*x_angle*y_angle +
bf*POWR(y_angle,2) + bg*POWR(x_angle,2)*y_angle +bh*x_angle*POWR(y_angle,2) + bj*s_y*POWR(y_angle,3)

  X_NA = (x_angle + x_NADelta/2)      #division of 2 because Optical angle is 2x mecahnical
  Y_NA = (y_angle + y_NADelta/2)

! This section inputs the X and Y angle into the Zemax Model
  SETSURFACEPROPERTY 3, PARM, X_NA, 3
  SETSURFACEPROPERTY 9, PARM, Y_NA, 3
UPDATE                                #this updates the Zemax file with the new angles
! This section finds the X and Y corrdinate of the beam
  CXtemp = OCOD("CENX")
  Xposition_c = OPEV(CXtemp, 16, 0, 1, 0, 10, 0)
  CYtemp = OCOD("CENY")
  Yposition_c = OPEV(CYtemp, 16, 0, 1, 0, 10, 0)

! This section outputs the X and Y position values
  OUTPUT "locationThor_C.txt", APPEND
  PRINT x_angle, ",", y_angle, ",", X_NA, ",", Y_NA,",", x_NADelta, ",", y_NADelta, ",", x_spot, ",",
y_spot, ",", Xposition, ",", Yposition, ",", Xposition_c, ",", Yposition_c
  !PRINT "X_Linear_A, Y_Linear_A, X_Corrected_A, Y_Corrected_A, X_Delta_A, Y_Delta_A,
X_Linear_P, Y_Linear_P, X_Distorted_P, Y_Distorted_P, X_Corrected_P, Y_Corrected_P"
Next
Next

```

End of Macro

Works Cited

1. **Marshall, Gerald.** *Optical Scanning*. New York : Marcel Dekker, Inc, 1991.
2. **McKinney, Michael.** Scanning Systems Help Laser Make Their Mark. *Photonics Spectra*. July 2003.
3. **Edmunds Optics.** *TechSpech F-Theta Scanning Lens*. Barrington : Edmunds Optics.
4. **Laikin, Milton.** *Lens Design*. 4th. s.l. : CRC, 2006. 978-0849382789.
5. **ULO Optics.** *MULTI-ELEMENT ZNSE SCANNING LENSES, ZSD-15 & ZST-15 SERIES*. Stevenage : ULO Optics Ltd, UK & Worldwide, 2015.
6. **Sintec Optronics.** *Optics for Laser Scanners*. Industry Report.
7. **Sasian, Jose.** *Introduction to Aberrations in Optical Imaging Systems*. New York : Cambridge, 2013. 978-1-107-00633-1.
8. *Geometrical Aberrations*. **Gross, Herbert.** 2016, Design and Correction of Optical Systems.
9. **Sacek, Vladimir.** 3. TELESCOPE ABERRATIONS: TYPES AND CAUSES. *TelescopeOptics.net*. [Online] June 2015. [Cited: June 9, 2016.] <http://www.telescope-optics.net/aberrations.htm>.
10. **Smith, Warren.** *Modern Optical Engineer*. New York : McGraw Hill, 2007. 0071593756, 9780071593755.
11. **Hassebrook, Laurence and Guan, Chun.** Distortion. [book auth.] Ronald G. Driggers. *Encyclopedia of Optical Engineering*. s.l. : CRC, 2003.
12. **Savard, John.** The Five Seidel Aberrations. *Introduction to Geometric Optics*. [Online] 2004. [Cited: May 22, 2016.] <http://www.quadibloc.com/science/opt0505.htm>.
13. **Schaub, Michael, et al., et al.** *Molded Optics: Design and Manufacture*. s.l. : CRC Press, 2016.
14. **Hecht, Eugene.** *Optics*. 4th Edition. San Francisco : Pearson Education, Inc, 2002. 0-8053-8566-5.
15. **Greivenkamp, John.** *Field Guide to Geometrical Optics*. Bellingham : SPIE Press, 2004. 0-8194-5294-7.
16. *Aberrations I*. **Gross, Herbert.** 2016, Lens Desig 1, p. 24.

17. **Kingslake, Rudolf and Johnson, R. Barry.** *Lens Design Fundamentals*. 2nd Edition. Burlington : Elsevier, 2010. 978-0-12-374301-5.
18. **Hugemann, Wolfgang.** *Correcting Lens Distortions in Digital Photography*. Leverkusen : EVU, 2010.
19. *A Simple Method of Radial Distortion Correction with Centre of Distortion Equation.* **Wang, Aiqi, Qiu, Tianshuang and Shao, Longtan.** 35, s.l. : Springer Science, 2009, Journal of Math Imaging and Vision. 105851-009-0162-1.
20. *Third-Order Aberration Coefficients of a Thick Lens.* **Miks, Antonin and Novak, Jiri.** 33, Prague : Applied optics, 2012, Vol. 51.
21. **II-VI Infrared.** II-VI Infrared Optic Materials. *II-VI Infrared*. [Online] 2016. [Cited: February 24, 2016.] <http://www.iivinfrared.com/Optical-Materials/znse.html>.
22. **IDEX.** Gaussian Beam Optics. *IDEX Support Documents*. [Online] [Cited: July 26, 2016.] https://marketplace.idexop.com/store/SupportDocuments/All_About_Gaussian_Beam_OpticsWEB.pdf.
23. **Rolland, Jannick and Hopkins, Terry.** *A Method of Computational Correction for Optical Distortion in Head-Mounted Displays*. Chapel Hill : Dept. of Computer Science, UNC.
24. **Czajkowski, Amber.** *Specifying an Aspheric Surface*. Tucson : s.n., 2007.
25. *Correction of Principles.* **Gross, Herbert.** 2016, Design and Correction of Optical Systems, p. 8.
26. **Saleh, Bahaa and Teich, Malvin.** *Fundamentals of Photonics*. Hoboken : John Wiley & Sons, Inc, 2007. 978-0-471-35832-9.
27. **Crystran.** Optical Materials. *Optical Materials Website*. [Online] 2012. [Cited: February 24, 2016.] <http://www.crystran.co.uk/optical-materials>.
28. *Femtosecond laser optics combat pulse dispersion, color errors, and reflections.* **TOESKO, GÜNTER.** March 18, 2016, Laser Focus World.
29. **Kingslake, Rudolf.** *Optical System Design*. New York : Academic Press, 1983. 0-12-408660-8.
30. **Newport.** Optics Fundamentals. *Newport Technical Notes*. [Online] Newport, 2016. [Cited: July 6, 2016.] <https://www.newport.com/optics-fundamentals>.
31. **Sutton, Michael A., Orteu, Jean-Jose and Schreier, Hubert W.** *Image Correlation for Shape, Motion and Deformation Measurements*. New York : Springer, 2009. 978-0-387-78746-6.